ABSTRACT

Title of Document:	THERMO-OPTIC ASPECTS OF LARGE SCREEN PLASMA DISPLAY PANELS
	Jeffry J. Kahn, MS, 2007
Directed By:	Professor Avram Bar-Cohen, Department of Mechanical Engineering

Plasma Display Panels (PDPs) are a popular technology for large size television displays. Screen inefficiencies, which result in significant localized heat generation, necessitate the use of advanced thermal management materials to reduce the peak temperatures and spatial temperature variations across the screen. In the current study, infrared thermography was used to obtain thermal maps of a typical, 42", high-definition PDP screen for different illumination patterns and for several configurations of externally controlled heaters simulating PDP heat generation. The results were used to validate a three-dimensional numerical thermal model of the PDP designed to predict the beneficial effects of anisotropic graphite heat spreaders on the temperature distribution. In addition, a color analyzer was used to determine the spatial and temporal variations in luminosity across the PDP when operated continuously for 1750 hours. The thermal model and experimental luminosity characteristics were used to evaluate the deleterious effects of temperature on PDP performance.

THERMO-OPTIC ASPECTS OF LARGE SCREEN PLASMA DISPLAY PANELS

By

Jeffry J. Kahn

Thesis submitted to the Faculty of the Graduate School of the
University of Maryland, College Park, in partial fulfillment
of the requirements for the degree of
Master's of Science
2007

Advisory Committee:
Professor Avram Bar-Cohen, Chair
Associate Professor Patrick McCluskey
Assistant Professor Bao Yang

Acknowledgements

Table of Contents

List of Tables

List of Figures

Chapter 1: Introduction

Plasma display panels (PDPs) are highly popular due to several key advantages over competing display technologies. PDPs can support very large screen sizes (up to 2.61m (103") diagonal) while maintaining a thin form factor (<4"). PDPs also have a fast response time, high uniformity of brightness and contrast, and a wide viewing angle that make the display excellent for video playback [1].

PDPs utilize an emissive technology that has a very unique method for producing light. An electric field triggers an ultraviolet discharge from the gaseous combination of xenon and neon stored in individual plasma cells. The ultraviolet light reacts with a phosphor layer in the discharge region to create red, green, and blue sub-pixels. The grouping of three sub-pixels creates one pixel, as shown in Fig. 1, which can be controlled and grouped in appropriate ways to produce images [2].
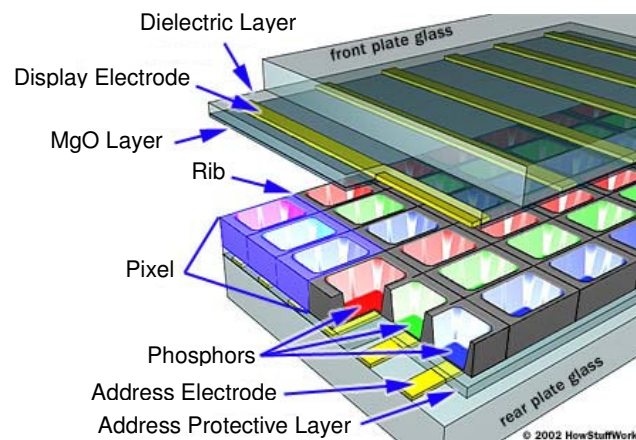
Fig. 1. PDP components [3].

PDPs are relatively inefficient, with a total conversion efficiency of approximately 1.5% [4]. With such low efficiency, and typical PDP power inputs of

300W, large quantities of heat are generated in the screen. One of the problems inherent in PDP technology is the presence of large temperature gradients on the screen. High temperatures and large temperature gradients are especially prevalent when the image on the screen is static and contains large white areas. Such a situation would commonly occur if the PDP was being used as a computer monitor. In order to create a white image, all three sub-pixels must fire simultaneously, creating a strong discharge that causes increased heat generation and higher temperatures in the white region.

Highly non-uniform temperature patterns are detrimental to PDP display quality because the total luminosity of the PDP decreases as the screen temperature increases. This research effort focused on reducing the peak temperatures and on-screen temperature variations through the use of anisotropic natural-graphite heat spreaders which were applied to the rear of the back panel of an operating commercial PDP [5, 6, 7]. To overcome uncertainty in the power dissipation distribution within the PDP and operating constraints associated with the PDP's power management protocols, externally controlled heaters attached to the back of the screen were used to simulate PDP heat generation patterns. IR imaging of the resulting temperature field was used to calibrate a numerical thermofluid model of the PDP. This model was then used to predict the beneficial effects of graphite heat spreaders on the temperature distribution of the PDP.

To further evaluate the detrimental effects of temperature on PDP performance, the externally controlled heaters were used to artificially elevate screen temperatures to determine a relationship between luminosity and temperature.

Additionally, a second PDP was operated continuously for 1750 hours to quantify the

effect of time on PDP performance at various screen fluxes.

Chapter 2: Fundamentals of Plasma Display Panels

How the Human Eye Operates

The eyes, suspended in the skull, are each moved by six extra ocular muscles attached to the tough, fibrous outer-coating of the eye, called the sclera (Fig. 2). The conjunctiva, a mucous membrane lining the eyelid, folds back to attach to the eye. The eye itself is a sphere approximately 2.5cm in diameter. The sclera, which is made up of closely interwoven fibers, appears white in color around the circumference of the eye. However, in the front-center, where the eye bulges out to form the cornea, the sclera is transparent to allow light to enter. Behind the cornea is a ring of muscles, called the iris. In the center of this ring is an opening called the pupil, which controls the amount of light entering the eye [8].

Beyond the pupil, light passes through the anterior chamber of the eye, to the lens. The anterior chamber is filled with a fluid, called the aqueous humour, which transports oxygen and nutrients to the eye and carries away waste products. The cornea and the lens alter the light passing though the eye so that it will be in focus on the back of the eye, which is covered by the retina. After passing through the lens, light passes through the main part of the eye which contains a clear, gelatinous substance called the vitreous humour. Finally, the light contacts the retina [8].

13. Canal of Schlemm
15. Conjunctiva
4. Ciliary body
12. Aqueous humor
2. Cornea
6. Pupil
14. Lens
5. Iris
1. Sclera
3. Choroid
7. Retina
Fovea
8. Macula
9. Optic nerve
10. Optic disc
11. Vitreous humor

http://health.howstuffworks.com/eye1.htm
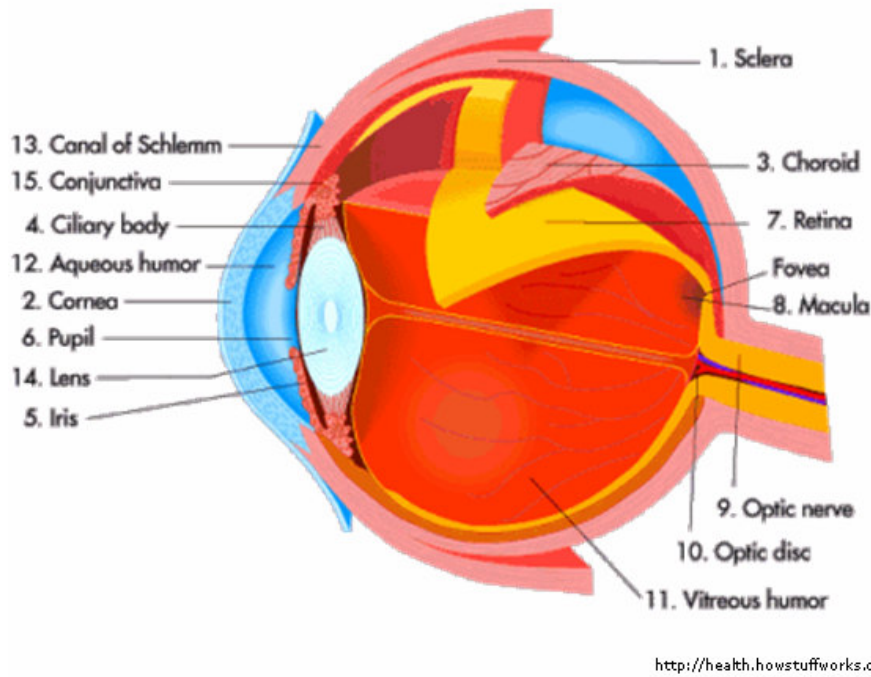
Fig. 2. Diagram of the human eye [2]

The retina is divided into three main layers—the receptor cell layer, the bi-polar layer, and the ganglion cell layer (Fig. 3). The receptor cell layer, located at the back of the retina, contains the photoreceptors that sense light. The photoreceptors form synapses with bipolar cells, which in turn synapse with the ganglion cells whose axons travel through the optic nerve to the brain. The axons come together and pass through the receptor and bipolar cell layer, exiting the eye at a point called the optic disc. The optic disc forms a blind spot in the eye; interestingly, human perception is not aware of this blind spot due to a phenomenon called "filling in." The retina also includes the outer plexiform layer, which transmits information in a direction parallel to the retinal surface, allowing for the combination and subtraction of messages from adjacent photoreceptors [8].
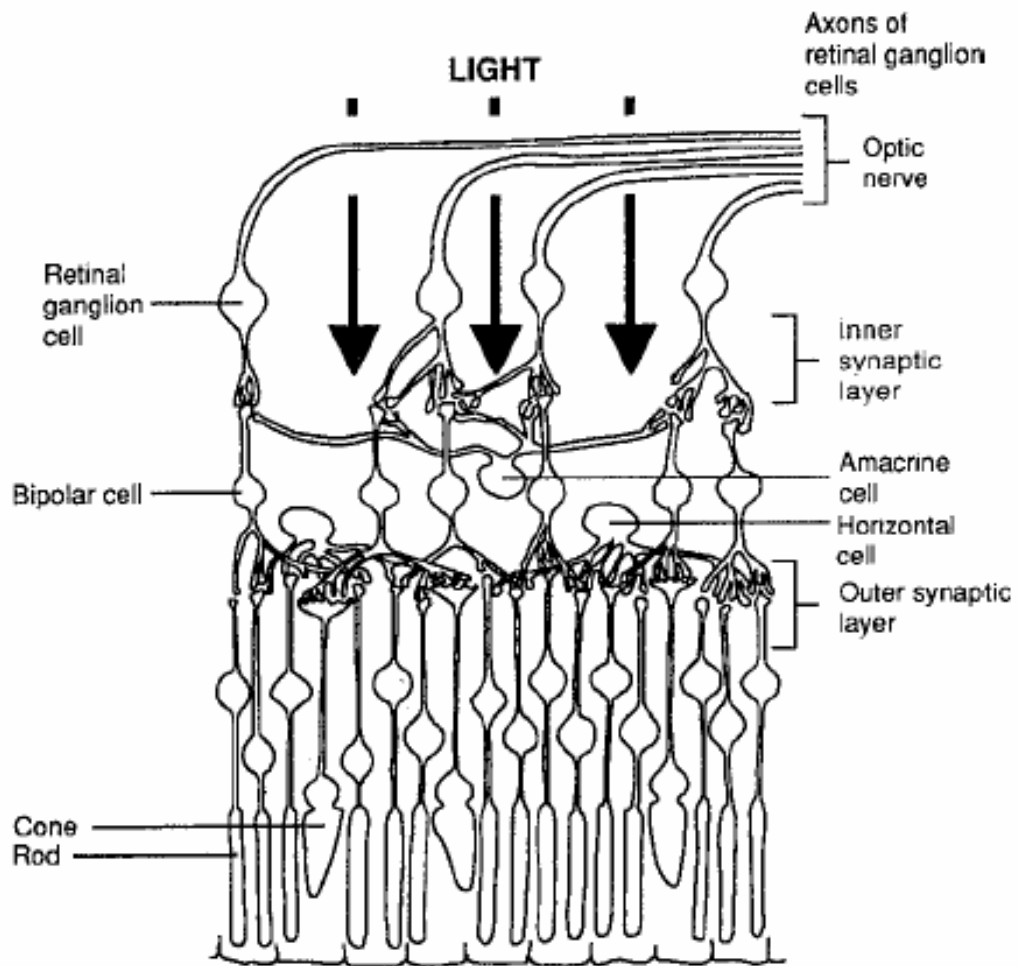
Fig. 3. The neural structure of the retina photoreceptors [8]

After the image is focused on the retina, the transformation from light to neural activity is carried out by the photoreceptors. There are two types of photoreceptors: rods and cones. The human retina contains approximately 120 million rods and 6 million cones, which are concentrated in a small area of the retina called the fovea. The cones mediate diurnal vision providing high-acuity color vision, while the rods mediate nocturnal vision and provide only low-acuity monochromatic vision [8].
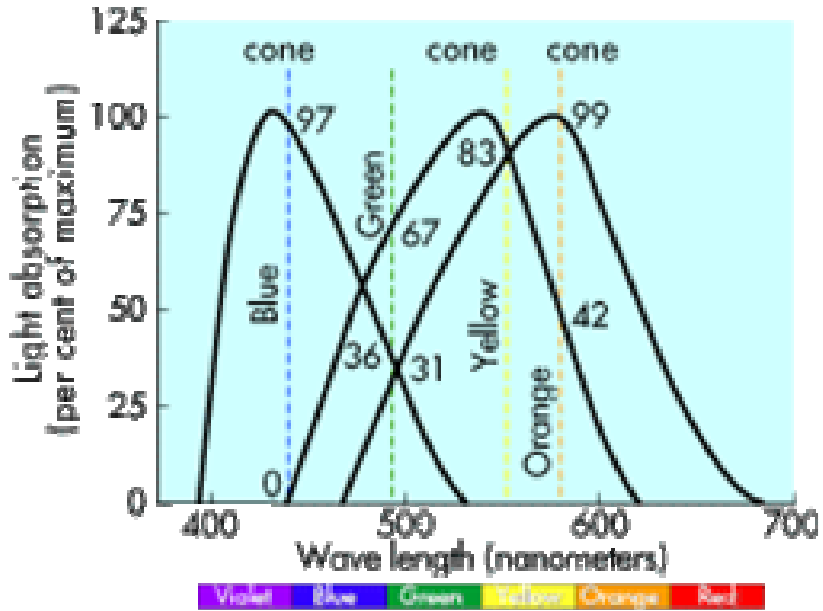
Fig. 4. Wavelength sensitivities of each cone type [2]

There are three types of cones in the eye. Between 5% and 10% of the total cone population are short-wavelength blue pigment cones, absorbing maximally at 420nm (Fig. 2). The blue cones form an annulus around the ring of the fovea. 40% of the cone population is green or middle-wavelength pigment cones, which absorb maximally at 530nm. The remaining 60% is red or long-wavelength pigment cones, absorbing maximally at 565nm [8].   The overall peak sensitivity of the eye to visible light, with wavelengths between 400 and 650nm, is at 555nm [2]. Human vision is unable to sense electromagnetic radiation outside of the visible range, shown in Fig. 5.   An energy conversion process is necessary if other wavelengths, such as ultraviolet, are to be perceived.
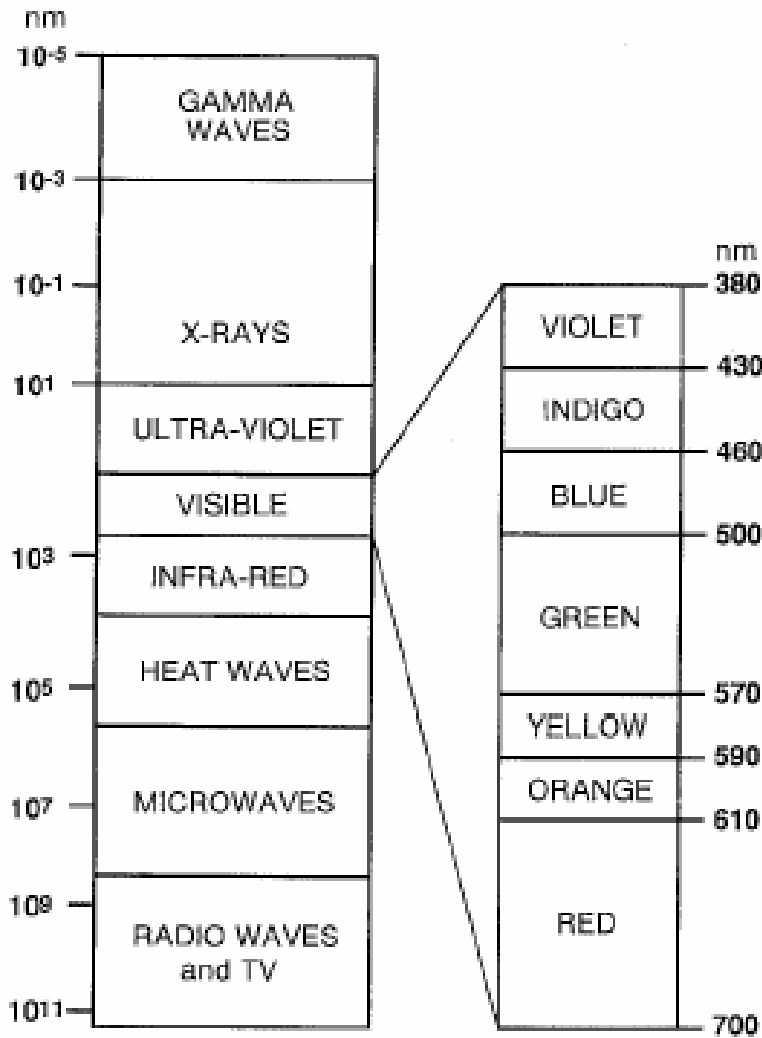
Fig. 5. Wavelengths of various forms of electromagnetic energy [8]

The three cone types are necessary to discriminate between colors because a single cone cannot differentiate between changes in wavelength and changes in intensity. For instance, a red cone will respond strongly to 560nm light, but weakly to 500nm light. The same response pattern can be obtained by using a fixed wavelength of light (e.g. 560nm) and varying the intensity. This is called univariance. As a result, a comparison of signals from two or more cone types is necessary to differentiate between wavelength and intensity—540nm and 640nm

lights will produce different patterns of firing in the red and green cones than two 540nm lights of varying intensity [8].

The eye makes use of three opposing mechanisms to interpret these cone responses. The first compares the differences between the responses from the red and green cone classes. The second compares the difference between the blue cone response and the sum of the red and green (yellow) cone responses. The final mechanism is an achromatic mechanism that detects differences in luminance. Remarkably, the visual system is able to detect changes in illumination of less than 1% [8]. In order to understand these mechanisms, a more detailed description of the light-to-neural activity process is needed.

When light enters the eye, it comes in contact with the photoreceptors. Photoreceptors consist of an inner segment and an outer segment, which contain the cell nucleus (Fig. 6). The outer segment contains roughly 750 thin membrane plates, called lamellae. In rods, the lamellae are free-floating discs, where in cones they consist of one continuous folded membrane. Embedded in the lamellae membrane is rhodopsin, the photopigment molecule. A single human rod contains 100 million photopigment molecules packed tightly together so that there is only 20nm of space between them [8].

A pigment molecule consists of two parts: opsin, a protein that is connected by a Schiff-base linkage to retinal, a lipid synthesized from vitamin A. Retinal is a long-chain molecule that can exist in two forms, or isomers: a straight-chain form, called all-trans retinal, and a bent form, called 11-cis-retinal. 11-cis-retinal is the only retinal form that can bind to the opsin. When the 11-cis-retinal absorbs a photon of

light, the long chain straightens to the all-trans form by a process called photoisomerisation. This causes the photopigment molecule to break into its two constituent parts [8].
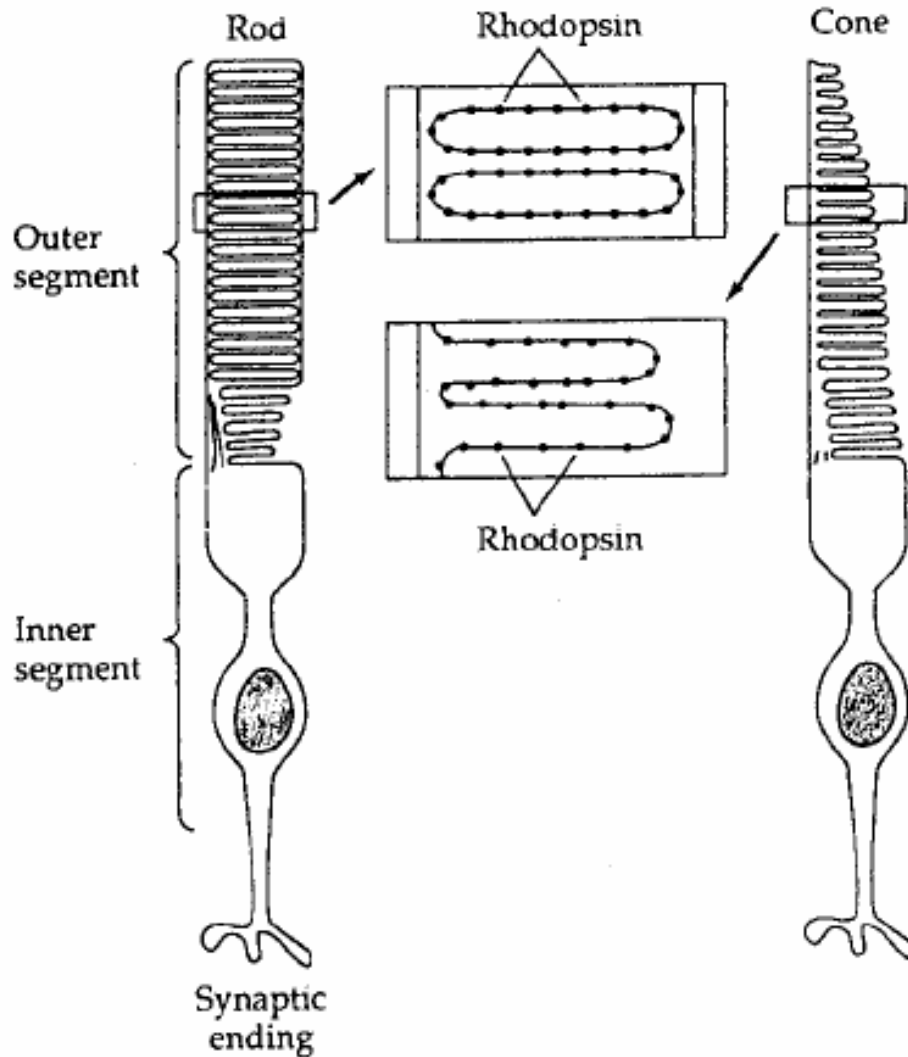
Fig. 6. Schematic diagram of the rods and cones [8]

In darkness, the rods and cones have a resting membrane potential of -40mV, considerably less than the usual membrane potential of -80mV. This is due to a continuous dark current that flows into the outer segment as sodium ions (Na^+) move down their electrochemical gradient through open cation channels. Incident light

causes hyperpolarisation of the cell membrane by indirectly closing the cation channels in the outer segment membrane. Cation channels are normally held open by cytoplasmic cyclic guanosine 3'-5'-monophosphate (cGMP). The photoisomerisation of the rhodopsin evokes a series of reactions that result in a rapid reduction in cGMP levels. This causes the cation channels to close and the electrical resistance of the outer segment membrane to increase, stopping the dark current. A single photon can close approximately 300 cation channels, roughly 3-5% of the open channels in darkness. Internal levels of cGMP fall about 20% upon illumination. The cGMP is effectively a messenger within the cell that transfers news of the incident light from the rhodopsin in the disc membrane to the ion channels in the cell membrane [8]. This entire reaction, from incident light to a perceived light, lasts less than a tenth of a second [2].

There are about 126 million photoreceptors in the retina, each signaling if light is absorbed at a particular point in the retina. This information is transmitted to the brain via the one million ganglion cell axons. Consequently, the retina must condense and reorganize the information from the photoreceptors into a form that can be transmitted to the optic nerve. The purpose of the visual system is not just to signal the presence or absence of light, but to detect patterns of light that can be used to identify objects and their spatial relationships in the external environment. The first step in this process is to detect differences in light at adjacent locations, which is likely to signal an edge or border that can be used to reconstruct a picture of the environment. Areas of uniform illumination are less important because they are unlikely to signal an edge [8].

Regional light differences are first extracted at the ganglion cells, which are connected to a number of photoreceptors via bipolar cells. Stimulating these specific photoreceptors, in what is called the receptive field, creates a corresponding ON response in the related ganglion cells, while simultaneously inhibiting the ganglion cells attached to surrounding photoreceptors to an OFF response. This allows the cells to respond to the orientation of the edge. The end result is that the orientation of a stimulus can be determined by comparing the responses of a number of ganglion cells [8].

	Intensity (candelas/m²)	
The sun at noon	10^{10}	Damaging
	10^9	
	10^8	
	10^7	
Filament of a 100W light bulb	10^6	
	10^5	
White paper in sunlight	10^4	Photopic vision
	10^3	
	10^2	
Comfortable reading	10	
	1	Mesopic vision
	10^{-1}	
White paper in moonlight	10^{-2}	
	10^{-3}	
White paper in starlight	10^{-4}	Scotopic vision
	10^{-5}	
Weakest visible light	10^6	

Table 1. Range of visible light intensities [8]

Relating back to vision and viewable light intensity levels, the human eye is able to see over a range of illumination levels of about $10^{10}-10^{12}$:1 (Table 1). However, the information leaving the eye travels along the optic nerve fibers, which

have a limited response range of 100:1. An enormous range of inputs must be mapped onto a very small range of outputs [8].

To deal with this, the eye adapts to various light intensities by changing the absolute luminosity threshold at which it senses incident radiation. A threshold is the faintest light that can be seen, on average about ten rods activated by photons of light. The absolute threshold changes as the eye adapts to darkness. Cones, with a minimum absolute threshold of 10^{-3} cd/m², take about 10 minutes to adapt to dark. Rods, with a minimum absolute threshold of 10^{-6} cd/m², take 25-30 minutes to adapt. During dark adaptation, the threshold is lowered until the stimulus is just seen— adaptation does not differentiate between rod and cone perception. This increase in visual sensitivity during dark adaptation is attributed to changes in the neural connections of the retina as the visual pigments regenerate [8].

There eye also has a threshold for determining differences in luminosity between two adjacent fields, which is roughly a 0.8% variation under optimum conditions. This threshold is important because it determines the human ability to see an object against a background. In terms of PDP performance, this threshold determines if nonuniformities in the display surface are perceptible. As mentioned above, the ganglion cells force receptors just outside of the areas activated by light to have an OFF response. This serves to enhance the borders between the two adjacent fields. However, the presence of a contour or sharp boundary between the two fields is essential if the fields are to be distinguished. A very gradual transition from high to low luminance might appear as a uniform field [8].

A typical Samsung plasma display panel (PDP) is composed of millions of three-part cells that are 1.08mm x 0.36mm x 0.15mm in size and produce a single pixel of an image [9]. Plasma displays create images from the controlled emission of fluorescent light by each of the pixels. Each pixel is composed of three fluorescent light "cells," each of which contains phosphors for red, green, and blue lights. Each cell can produce one of 256 different light intensities, meaning that an individual pixel can produce roughly 16.8 million distinct colors. Intensities are not adjusted by a change in applied voltage or current, but rather by the amount of time that the cell is actually discharging light. The human eye, with its much slower perception speed, discerns this as intensity [10].

The PDP cells are enclosed between two glass plates on the front and back ends of the display. Barriers are positioned to separate the individual cells, and the entire enclosure is sealed along the outer edges to maintain a predetermined pressure and gas mixture between the plates. The gas mixture is generally a combination of Xenon with another noble gas, such as Helium or Neon, and pressure is generally set at approximately one-half of atmospheric pressure [9].

The central element in a PDP is the plasma, a gas made up of free-flowing ions (positively charge atoms) and electrons (negatively charged particles). Under normal conditions, a gas is mainly made up of uncharged particles—the net electric charge of each particle is zero. However, when free electrons are introduced into the gas by establishing an electrical potential across it, the situation rapidly changes. The free electrons collide with atoms knocking loose other electrons. An atom missing an

electron now has a net positive charge, making it an ion. When a current is applied to the plasma, the negatively charged particles are attracted toward the positively charged electrode, while the positively charged particles flow toward the negatively charged electrode. Particles are constantly bumping into each other during this mass migration. The collisions between positively charged ions and electrons further "excite" the xenon and neon gas atoms in the plasma, causing them to jump to a higher energy state. When these gas atoms fall back to their original energy states, they release the extra energy in the form of ultraviolet light photons [11].
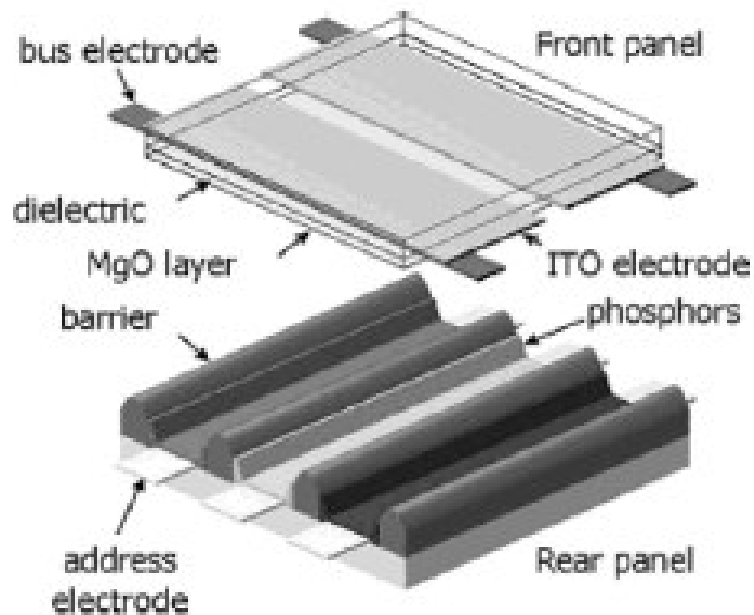
Fig. 7. Structure of a PDP pixel [2]

In a typical 42" high-definition PDP, 930 cm by 530 cm in outer dimension, the xenon and neon gas is contained in approximately 1.25 million cells sandwiched between the two glass plates (see Fig. 7). The address, or bus, electrodes are located behind the cells along the rear glass plate. The transparent display electrodes are mounted above the cell along the front glass plate, and are surrounded by an

15

insulating dielectric material and covered by a magnesium oxide (MgO) protective layer, which also assists in secondary electron emission. Both sets of electrodes extend entirely across the screen. The display electrodes are arranged in horizontal rows along the screen and the address electrodes are arranged in vertical columns, forming a basic grid. To ionize the gas in a particular cell, the electrodes that intersect that cell are charged by creating a voltage difference between them, causing an electric current to flow through the gas in that particular cell and stimulating the gas to release ultraviolet photons [10]. If this is done repeatedly with many cells (pixels) across the entire PDP, an image can be sustained [11].
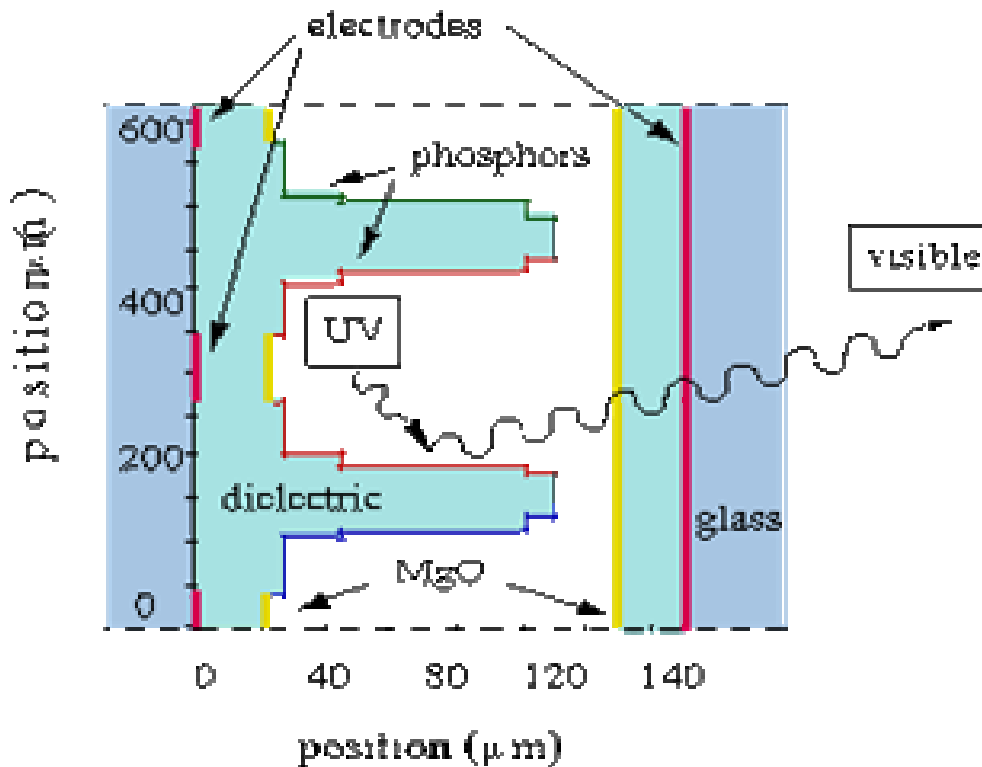
Fig. 8. Cross-sectional view of a PDP pixel [9]

Since the ultraviolet photons generated by the plasma are not visible to the human eye, use of this technology for information displays requires conversion of this energy to the visible spectrum. In PDPs, this energy conversion is accomplished by having the ultraviolet radiation interact with phosphor materials coated on the inside wall of the cell (see Fig. 8). Phosphors are substances that release light when they are exposed to a different type of light. When an ultraviolet photon interacts with a phosphor in the cell, one of the phosphor's electrons jumps to a higher energy level. When the electron falls back to its normal level, it releases energy in the form of a visible light photon. The specific phosphors used in a PDP— $BaMgAl_{10}O_{17} : Eu^{2+}$ (BAM) for blue emission, $Zn_2SiO_4 : Mn^{2+}$ (ZSM) for green emission, and $(Y,Gd)BO_3 : Eu^{3+}$ (YGB) for red emission—give off colored light when they are excited [11].

History

The plasma display panel was invented in 1964 by Bitzer, Weber, and Slottow at the University of Illinois. The panel had only a single cell, but operated using the same fundamental principles that govern today's high definition PDPs. That same year, the researchers were able to create a 16x16 panel of independently controlled cells [12].

Throughout the 1970's, many large companies, such as IBM, RCA, Zenith, and General Electric, saw the potential in the technology and sponsored continued research. In 1983, the IBM 3290 Information Panel was released. It was, "the industry's first mass-produced, large-screen plasma display terminal for commercial use," according to an IBM advertisement. Other PDPs were also being used outside

of the commercial arena, in nuclear attack submarines and in the "Doomsday Plane," as command displays [12].

However, due to the extreme costs required to make plasma displays competitive with cathode ray tubes, almost all major TV and computer companies had given up on the technology by 1987. Only the Pentagon still supported a small but very lucrative plasma display industry [12].

In 1990, the University of Illinois founded Plasmaco, a company, led by Weber, dedicated to commercializing plasma display technology. By 1993, with the advent of liquid crystal displays, Plasmaco was in a dire financial state because it had yet to produce a commercially-viable color plasma display. Finally, on the last day of the 1994 display industry convention, Weber unveiled a PDP that displayed colored stripes and that was able to impress people with its brightness and contrast ratio. By 1999, Plasmaco had created a 60-inch PDP with the best contrast ratio of any large television display. Due to its high contrast ratios, high brightness, large viewing angles, slim form-factor, and ability to scale to large screen sizes, PDP technology has become very successful in today's marketplace [12].

Effect of Temperature

Increased temperatures during the life cycle of the PDP have been shown to significantly degrade the emission intensity and color accuracy of the blue phosphor (BAM), as well as negatively affect the YGB and ZSM phosphors to a lesser extent [13]. At higher temperatures, the population density of phonons is increased. Consequently, the full width at half-maximum (fwhm) of the three emission bands is increased with temperature (Fig. 9a) [14].

The peak positions of the emission spectra for all three phosphors are also blueshifted with increasing temperature, as shown in Fig. 9b. Elevated temperatures cause electrons at lower energy levels to jump to higher energy levels by phonon-assistance. As a result, nonradiative transitions from excited states to the ground state are prevented. The height of the higher-energy emission peak is increased and the height of the lower-energy emission peak is subsequently decreased. As a result of the convolution of these peaks, the blueshift behavior is observed [14].

The emission intensities of the three phosphors are also decreased with increasing temperature. The emission intensity is "thermally quenched" at higher temperatures, in the order of the blue, green, and then red phosphors. The quenching temperatures at which the initial peak intensity is halved are 270K for the blue phosphor, 360K for the green phosphor, and over 400K for the red phosphor. This effect is shown in Fig. 9c. Remember that UV radiation is only released when the electrons fall from the elevated energy state to the ground state. At higher temperatures, a larger percentage of the electrons are at higher energy states and do not fall back to the ground state during the discharge period. Consequently, the result is a decrease in emission intensity [14].

Additional temperature effects, such as decreased activation energy and MgO degradation are thoroughly discussed in future sections.
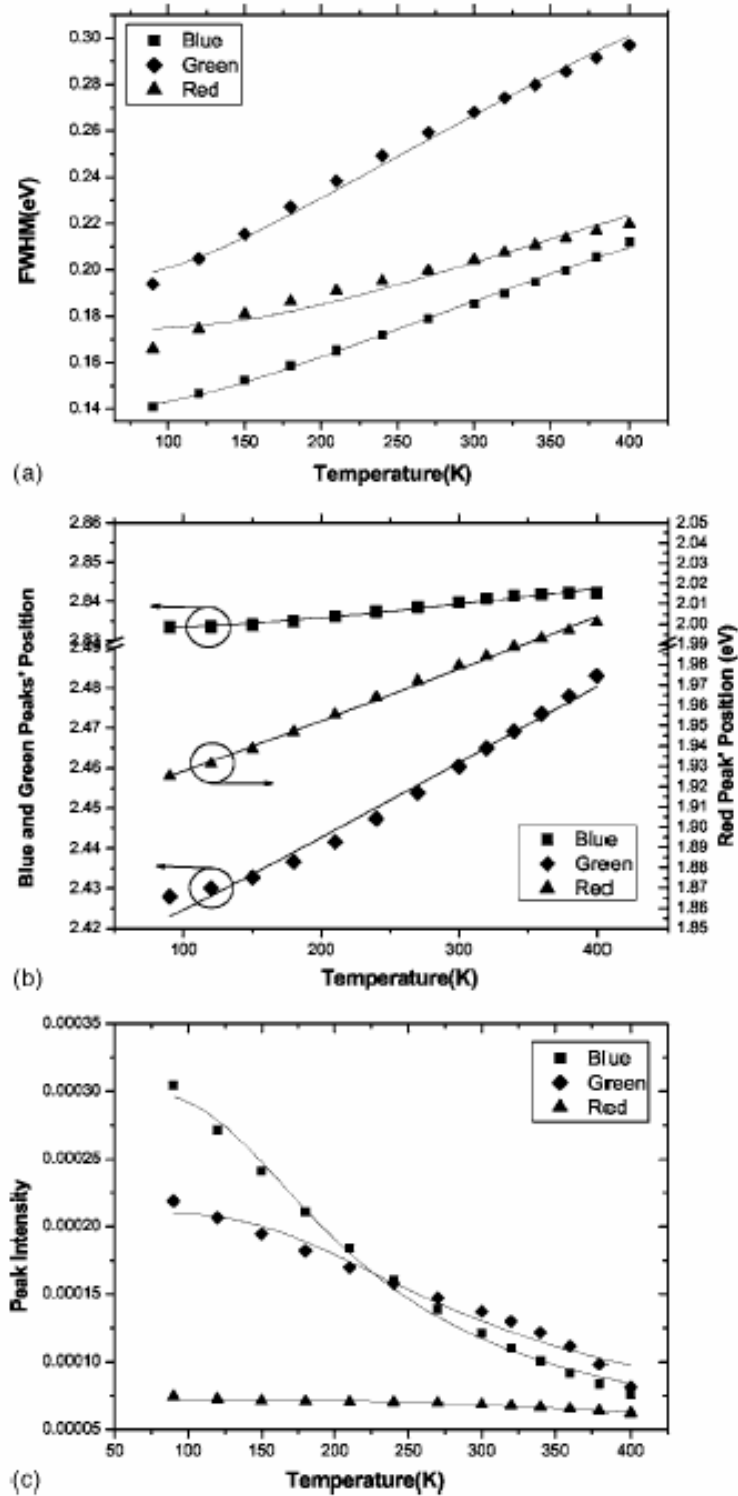
Fig. 9. (a) Emission bandwidths, (b) peak positions, and (c) emission intensities of BAM, ZSM, and YGB phosphors for various temperatures [14]

Effect of Time

Energetic ions, which are accelerated by the high electric field in the PDP, frequently collide with neutral atoms in the gas. When ions and neutral atoms with energies above a certain threshold (~55eV) collide with the MgO surface, they can damage the surface through the ejection of atoms. Although MgO is quite resistant to this form of damage, called sputtering, aging due to sputtering cannot be avoided. The purpose of the MgO layer is to protect the dielectric layer above the electrodes from sputtering while simultaneously assisting with secondary electron emission for the xeon/neon gasses. The MgO layer plays an essential role in keeping the operating voltage relatively low and in limiting damage due to sputter. Degradation of the MgO layer has both efficacy and lifetime consequences [15].

It is possible to predict the sputtering rate and the resulting lifetime if the sputtering yield, Y, and the flux energy distribution, F, is known for each particle (e.g. Xe^+, Xe, Ne^+, Ne). The ion and neutral flux energy distributions at the MgO surface are generally calculated by use of a numerical fluid model performing a Monte Carlo simulation of the ion and neutral atom trajectories from their position at birth to their arrival at the surface. The sputtering yield is defined as the number of sputtered particles per incident particle. Y is a function of the energy, angle of incidence, and mass of the incident particle, but it does not depend on the charge. For normal angles of incidence, the number of particles sputtered from the MgO surface per unit area during once current pulse (discharge), φ, is the product of the sputtering yield and the flux energy distributions integrated over energy and time and summed over all incident particles

$$\varphi = \sum_{k=1}^{2} \iint Y_k(E)\left(F_{k,ions}(E) + F_{k,neutrals}(E)\right) dEdt$$

where k = 1 for xenon and k = 2 for neon. Once φ is known, the sputtering rate, R, is found to be $R = \varphi \dfrac{M_{MgO}}{N_A \rho_{MgO}}$, where M_{MgO} and ρ_{MgO} are the atomic mass and mass density of the MgO, respectively. N_A is Avagadro's number. Neglecting any redeposition of the MgO, the MgO layer lifetime is, for a given thickness, d, and a frequency, f, $lifetime = \dfrac{d}{2fR}$ [16].

Several factors influence the lifetime of the MgO. Research has shown that lifetime increases with increasing the Xe concentration in the mixture, up to a 20% concentration. At this mixture ratio, the Xe and Ne fluxes carry approximately equal amounts of total energy, and are best able to balance out their respective ionic fluxes. Increasing gas pressure, up to .6atm, decreasing the voltage, and decreasing the dielectric capacitance also lead to increases in MgO lifetime [16]. Additionally, it can be presumed that operating at increased temperatures would decrease MgO lifetime because the lower breakdown voltage at the raised temperature causes the discharge to last for a longer time period, allowing for a higher probability that an energetic particle will damage the MgO.

Note that the MgO layer plays an essential role in keeping the operating voltage relatively low (due to secondary electron emission) in addition to limiting sputtering damage. Damage to the MgO layer has consequences relating to both the lifetime and efficacy of the PDP. Also, as the efficacy drops, additional power is

required to maintain constant a luminous output, resulting in an additional temperature rise [7].

Additional time-based degradation also occurs in the phosphors. The red phosphor, YGB, is the least susceptible to this effect, followed by the green (ZSM) phosphor and then the blue (BAM). Overall white luminance tends to decrease at a rate somewhere between the rates of the ZSM and BAM phosphors. These effects are shown in Fig. 10 [17]. The primary mechanism for this observed loss of efficiency is the formation of color centers in the spinel ($MgAl_2O_4$) blocks of the host. These defects provide a non-radiative pathway for the dissipation of absorbed UV radiation. This effect is significantly more pronounced in the BAM phosphor, which is susceptible to forming spinel-like states when excited by 120nm to 150nm wavelengths. Some of this energy is transferred to Ba states, yielding self-trapped excitons, and some is transferred non-radiatively to Eu^{2+} [18].
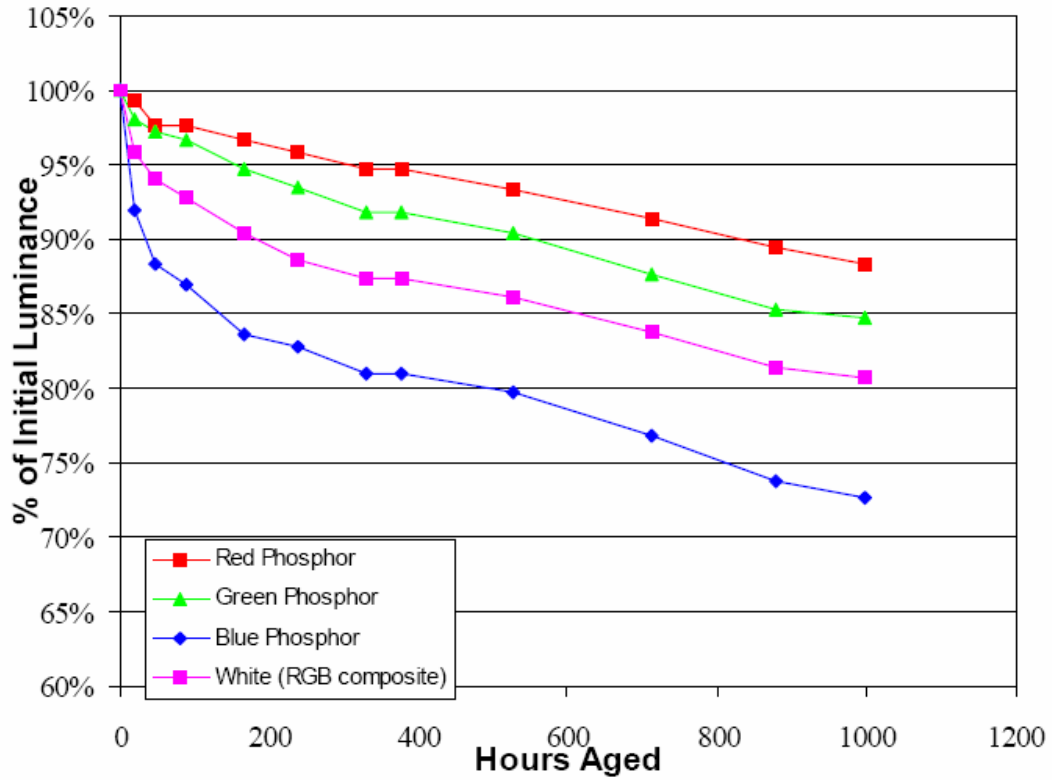
Fig. 10. Aging results for a typical Planar PDP [17]

Image Persistence

The full or partial persistence of an image, generated at a specified time, beyond its intended duration leads to a temporary deterioration in the quality of the PDP display. This phenomenon has been found to occur when the screen image is rapidly changed from a previous recurring pattern, typically displayed repeatedly for a short period of time (~5 minutes), to a subsequent dark or bright background [4].

24

(a) Original image pattern

(b) Dark background   (c) Bright background
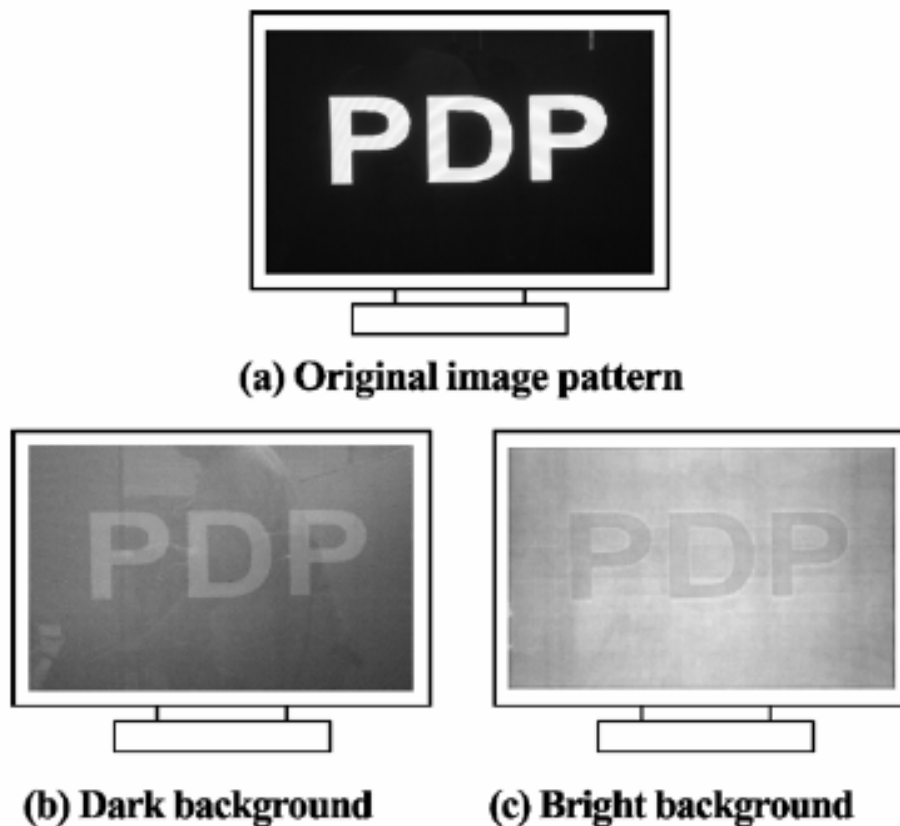
Fig. 11. (a) 'PDP' image continuously displayed for short period, (b) persisting 'PDP' image brighter than dark background, and (c) persisting 'PDP' image dimmer than bright background [4]

When the subsequent image is dark (Fig. 11b), image persistence causes a ghost image of the previous image that is brighter than the background. Since the luminance of the dark image is only produced by the weak reset discharge, the higher luminance of the ghost image is due the lower breakdown voltage in the heated gas and sustained activation of the heated MgO surface. The lower breakdown voltage of the gas causes a longer discharge which results in increased luminance [19,20]. Conversely, when the subsequent image is bright (Fig. 11c), image persistence creates a ghost image that is darker than the background. In this case, since the luminance of the subsequent bright image would be produced by the strong sustain discharge, the

25

lower luminance of the ghost image is due to the degradation of the phosphor layer. Phosphor layer degradation can be directly related to the cell temperature [19].

Energy Conversion Efficiency

An estimate of the energy balance in a typical PDP discharge is shown in Table 2. The first line states that only 40% of the energy dissipated in the discharge is used for electron heating. The most significant loss in efficiency, which is due to ion heating, is in this stage [7].

Secondly, only about half of the energy dissipated by the electrons in the discharge is used to excite the xenon. The rest of the energy is dissipated in the ionization of xenon and neon, and in the neon excitation, which only emits small amounts of UV. Fortunately, xenon is a very efficient UV emitter, and a large portion of the energy stored in the xenon ends up as UV photons. There is a 50% loss in efficiency during this stage [7].

Third, based on the cell geometry, an estimated 50% of the UV photons are lost on the front substrate where there is not phosphor. Next, despite the quantum efficiency of the phosphors being between 80% and 95%, the UV photons are not as efficiently converted into visible photons by the phosphors due to the large difference (~ a factor of 3) between the energy in the UV photons (~147-180nm) and the visible photons (~400-700nm). Approximately 25% of the remaining energy is lost during this conversion [7].

Finally, assuming that 60% of the visible photons leave the screen, a typical PDP has an energy conversion efficiency of only 1.5% [4].

Energy	%	Loss
Electric energy dissipated in discharge	100	
	↓	60% in ion heating (from models)
Energy dissipated in electron heating	$\rho = 40$	
	↓	50% in xenon ionization, neon excitation and ionization (from models)
Energy dissipated in xenon excitation	$\eta_{Xe} = 20$	
	↓	25% transition loss (e.g. infrared emission), quenching (from models)
Energy dissipated in UV production	$\eta_{UV} = 15$	
	↓	50% VUV photons not collected by phosphors (estimation)
UV energy reaching the phosphors	7.5	
	↓	67% UV to visible photon energy conversion loss (estimation)
Visible photons production	2.5	
	↓	40% visible photons not collected on front face (estimation)
Photons reaching the user	1.5	

Table 2. Estimated energy balance of a PDP discharge. The percentage in the second column is with respect to the total electric energy dissipated in the cell. The percentage given in the third column corresponds to the energy loss between two successive items in the first column [7].

However, considering the inefficiencies in the control electronics, the total luminous efficacy (power input to visible photons exiting screen) is less than 1%. Consequently, the luminous efficacy of a PDP, defined as the ratio of visible radiation or luminous flux to power input, is also very low. Typical luminous efficacies are on the order of 1-2 lumens/watt for currently produced PDPs. Laboratory prototypes have shown luminous efficacies of 3-5 lumens/watt [7].

It is possible to calculate the luminous efficacy of a PDP by measuring the luminous output from the screen and comparing it to the power input. First, it is necessary to define the units of light measurement, which are adjusted for the spectral response of the eye.

- A *candela* is defined as the luminous intensity of radiation at 555nm that has a radiant intensity of 1/683 watt/steradian. Fig. 12 reveals the value of 1/683 watt/steradian to correspond to the luminous efficacy of the human eye at peak of the sensitivity of photopic vision [21].
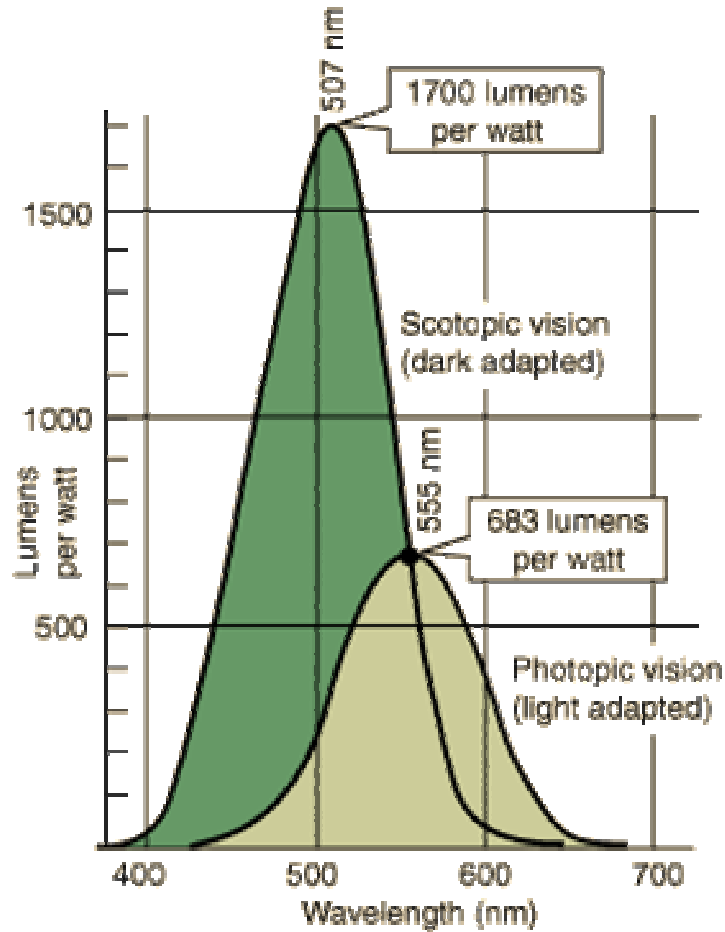
Fig. 12. Luminous efficacy of human vision [21]

- The *radiant flux* is defined as the energy per unit time radiated from a source over all visible wavelengths

- A *lumen*, the SI unit of luminous flux, is the measure of the weighted average of luminous flux radiation from a light source over all visible wavelengths

  o Lumen = radiant power x 683 lumens/watt x luminous efficacy

  o Lumen = luminous intensity (candela) x solid angle (steradian)

- *Luminous efficiency* is defined as the power efficiency of a light source

  o Luminous flux (lumens) divided by 683 lumens/watt

28

- *Luminous efficacy* is defined as the power efficiency adjusted for the spectral response of the eye

  o Luminous flux divided by (radiant flux times 683 lumens/watt)

It is now possible to determine the overall power efficacy of a PDP with a uniform screen pattern:

$$\text{Screen Efficacy} = \frac{\text{Luminous Intensity (cd/m}^2\text{)} * \text{Screen Area (m}^2\text{)} * \text{Solid Angle (sr)}}{683 \, \text{(lm/W)} * \text{Input Power to PDP (W)}} * 100\%$$

A calculation of the overall power efficacy of the PDPs used in this experiment yielded efficiencies on the order of 0.6%. Note that this value is the total efficacy of the entire unit, while the 1.5% value reported in Table 2 was only for power inputted to the plasma cells. If the data in Table 2 included losses in the control electronics, the two efficacies would be similar.

Chapter 3: Experimental Apparatus & Procedures

Introduction

Plasma display panels, with low conversion efficiencies and high power dissipations, have the tendency to generate large quantities of heat and large temperature gradients on the screen. The application of natural graphite heat spreaders to mitigate temperature gradients and possibly reduce operating temperatures was investigated. Since the application and removal of these spreaders is very labor and time intensive, a numerical model was created to predict screen temperatures for various spreader geometries and thermal conductances. To assist with the model calibration, externally controlled heaters were installed in a PDP to help determine power input to the screen. The heaters were also used to independently control the screen temperature to identify the relationship between temperature and luminosity. Finally, a second stock PDP was operated continuously for 1750 hours to determine the effect of time on screen performance.

PDP Test Vehicle

Two 42" Samsung HP-P4621 widescreen high-definition plasma display panels were utilized as the test vehicles for all experiments. These PDPs have a native pixel resolution of 1,024 x 768, a 16:9 aspect ratio, and allow for a VGA input. Samsung advertises that these screens have a contrast ratio of 3,000:1 and a brightness of 1,000 cd/m². The screens have a 50,000 hour lifetime, which is generally accepted by industry to be the point where the luminosity is 50% of the original value. Maximum power consumption is 380 watts [22].

30

Stock, factory standard PDPs from Samsung contain a natural-graphite heat spreader provided by GrafTech International. This spreader, of an indeterminate conductance, consisted of three separate sections, as shown in Fig. 13. Dimensions of the stock PDP are shown in Table 3.
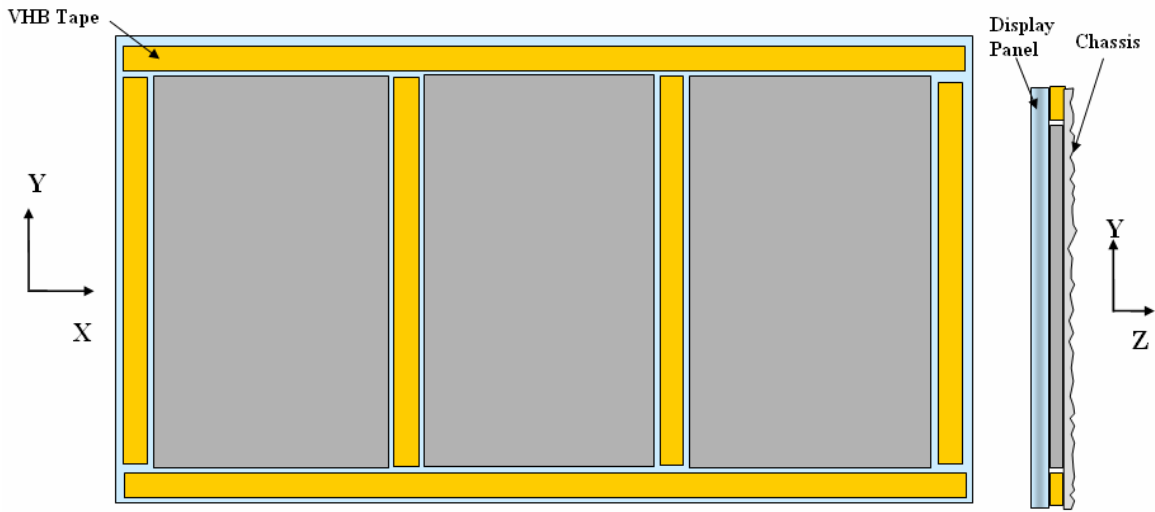
Fig. 13. View of spreader arrangement in un-altered PDP

	Height (mm)	Width (mm)	Depth (mm)
Glass	960	580	6
Visible part of glass (from front)	955	530	6
Active region, covered with pixels	930	530	6
Air gap between glass and chassis	960	580	1.4
VHB tape	----	25.4	1.5 (compressible)
Graphite heat spreader	525	280	0.95

Table 3. Physical dimensions of stock PDP

The stock PDP is also retrofitted with an electromagnetic interference shield (EMI). The EMI shield protects surrounding electronics from any electromagnetic radiation generated by the gas ionization process. The EMI shield is highly reflective and interfered with attempts to get accurate IR temperature measurements of the PDP screen. As a result, the shield was removed for all tests and analysis.

Thermal Spreaders

A 42-inch Samsung HP-P4261 PDP was retrofitted with several natural-graphite heat spreaders of various dimensions and thermal conductivities (Table 4). The natural graphite material used in these tests was eGRAF® SPREADERSHIELD™ † provided by GrafTech International Ltd. Each spreader, which featured an adhesive layer on one side, was applied to the rear of the back panel within the PDP (Fig. 14), and the resulting temperature and luminosity distributions were measured in the manner described in subsequent sections. An image of the spreader geometry is shown in Fig. 15.
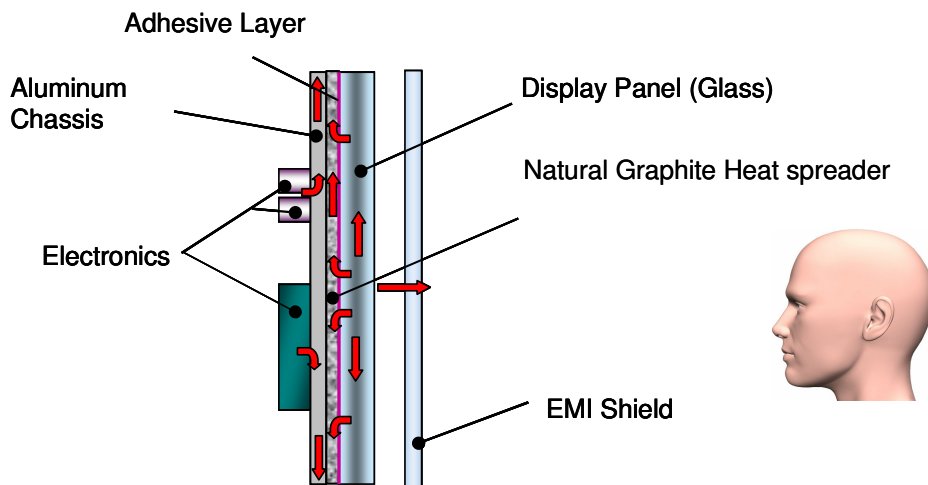
Fig. 14. Side view of PDP[23]
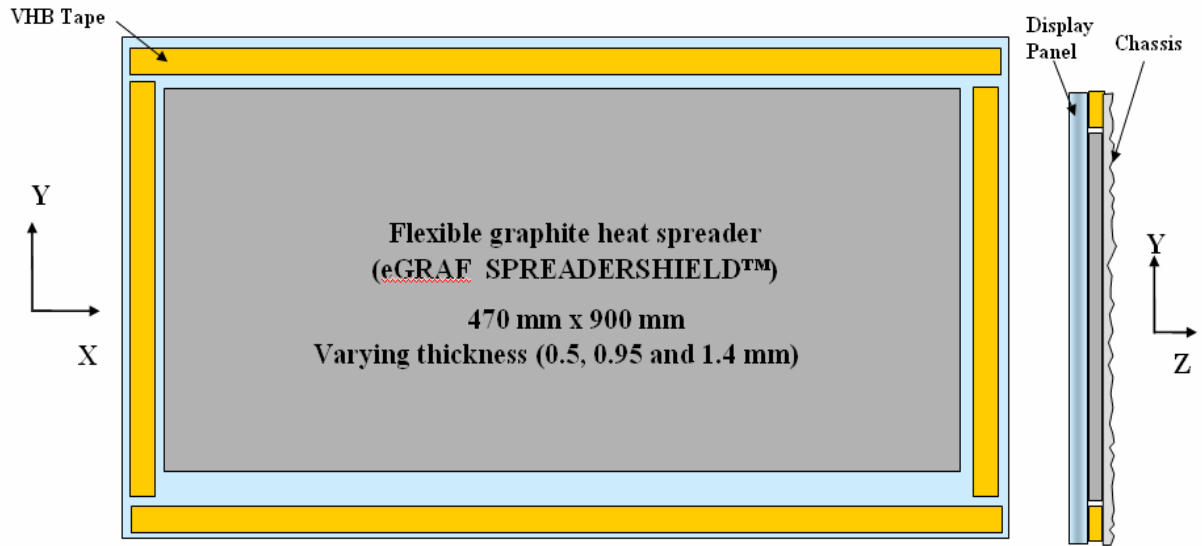
Fig. 15. Geometry of modified spreader. Dimensions of spreader were 470mm x 900mm, located40mm from the top of the glass [23].

Test Procedure

For each PDP-spreader configuration, measurements were performed for four different screen illumination patterns. Each pattern, created using a laptop computer with a VGA connection, consisted of a white square centered on the screen, as shown in Fig. 16, with screen loadings equal to 0 percent, 10 percent, 20 percent, and 100 percent. White-colored square boxes were used because the color white creates the most heating due to the activation of all three pixel colors. The screen loading was defined as the ratio of the illuminated area covered by the active pixels (A_w) to the total area of the screen (A_t). These specific screen loading values were chosen to reflect the wide range of illumination patterns typically seen in common television and movie films. A justification of the validity of these patterns is presented in the Experimental Results section on PDP power consumption. Irregardless, these patterns are artificial reconstructions.

33

Lateral Conductance (W/K)	$k_{xx}=k_{yy}$ (W/mK)	k_{zz} (W/mK)	Thickness (mm)
0.07 (Low)	140	10	0.5
0.29 (Intermediate)	305	5	0.95
0.616 (High)	440	5	1.4

Table 4. Heat spreader properties
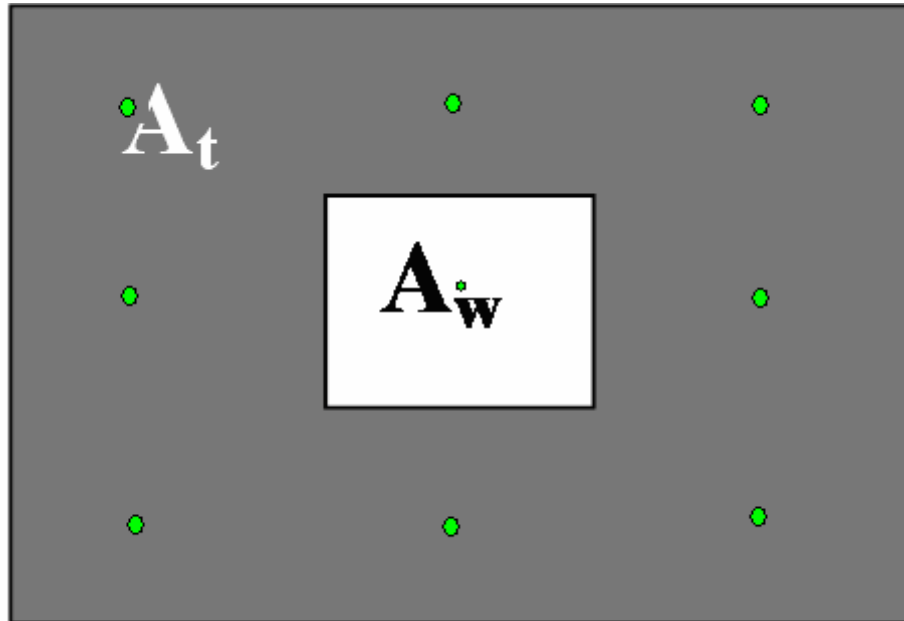
Fig. 16. PDP illumination patterns

Infrared thermography was used to determine the temperature profile on the screen. A ThermaCAM Merlin IR camera with a thermal sensitivity of 0.025°C, an accuracy of ±2C or ±2% of the reading, and a resolution of 320x256 was employed. The Merlin IR camera contains an auto-calibration feature, and automatically adjusts the calibration files to reflect the temperature ranges viewed by the camera. The camera was located roughly three meters from the PDP, and any additional sources of

radiation in the room were covered with black cloth to prevent IR reflections. The emissivity of the screen was determined to be 0.93 based on the material properties of the specific glass in the PDP.   Additionally, 10 thermocouples, shown as green dots in Fig. 16, were used to calibrate the IR camera and to provide temperature readings on the exterior of the chassis. The experimental setup is diagramed in Fig. 17.
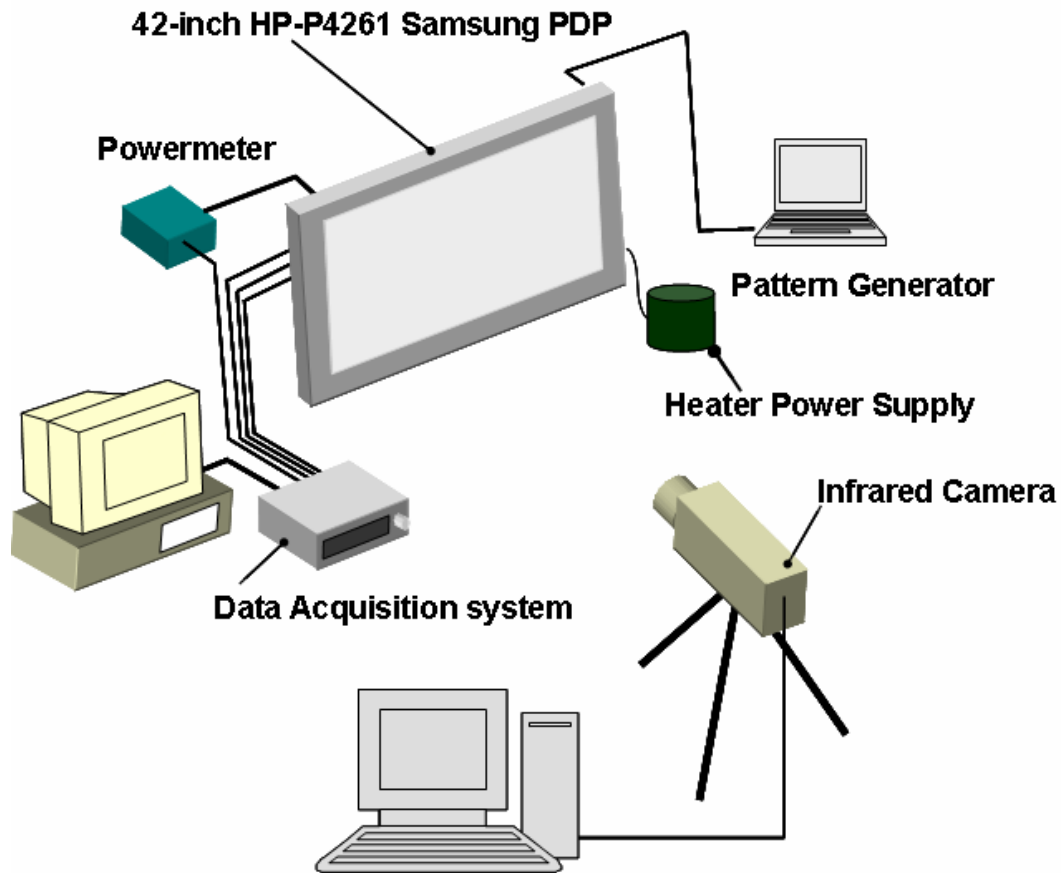
Fig. 17 Experimental setup and measurement system [24]

The reported thermal maps of the PDP screen and the temperatures at specific PDP locations were obtained when thermal steady-state conditions were attained, typically requiring three hours of operation at the specified illumination profile. Steady-state conditions were assumed when the average PDP temperature was

constant for a thirty minute period. All measurements were performed with the EMI shield removed.

Power input to the PDP was measured with a watt transducer from Ohio Semitronics, model PC5-001C, with a 0-500W input range, a 0-10V output, and an accuracy of ±0.5%.

Heater Array

For the externally-heated thermal imaging if the 42-inch Samsung HP-P4261 PDP, three Kapton insulated flexible heaters—a central square (10% screen loading) and two annular rings (sized to complete the 20% and 100% screen loading patterns)—were attached to the back panel of the display with an FEP adhesive. The heaters, Omega Engineering KH Series, had a maximum operating temperature of 120°C and a maximum heat flux of 7750 W/m². To aid in the analysis and interpretation of the observed temperature distributions, the heaters were designed to replicate the four screen loading patterns described above, i.e.0%, 10%, 20%, and 100%. Separate power supplies—three 1400W variable autotransformers—allowed each heater to be controlled independently. A thin (1/8" thick, 3.175mm) layer of foam insulation, installed with a thin layer of 3M spray adhesive, was used to fill the air gap within the PDP and to minimize heat transfer between the heaters and the electronics. A side view of this apparatus is shown in Fig. 18 [24].
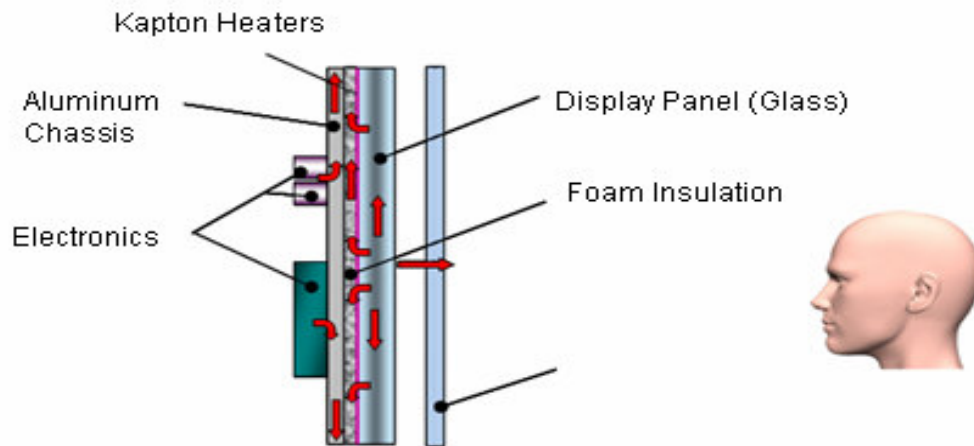
Fig. 18. Side view of PDP[24]

<u>*Luminosity Measurements*</u>

A Konica Minolta CA-210 display color analyzer was utilized to perform luminosity measurements. This color analyzer has an accuracy of ±0.002 for white chromaticity and can measure a luminance range of 0.1 to $1000cd/m^2$, spanning the expected luminance range of the PDP screen. A zero-calibration was performed prior to the start of each experiment. The color analyzer was employed in four distinct types of tests: a lifetime test, a temperature–luminosity dependence test, a luminosity–screen loading dependence test, and an image persistence test.

<u>Lifetime Test</u>
A second 42-inch Samsung HP-P4261 PDP was statically illuminated for 1750 continuous hours in order to quantify the temporal dependence of luminosity. The illumination pattern for this test, displayed on the PDP via the VGA output from a laptop, is shown in Fig. 19.
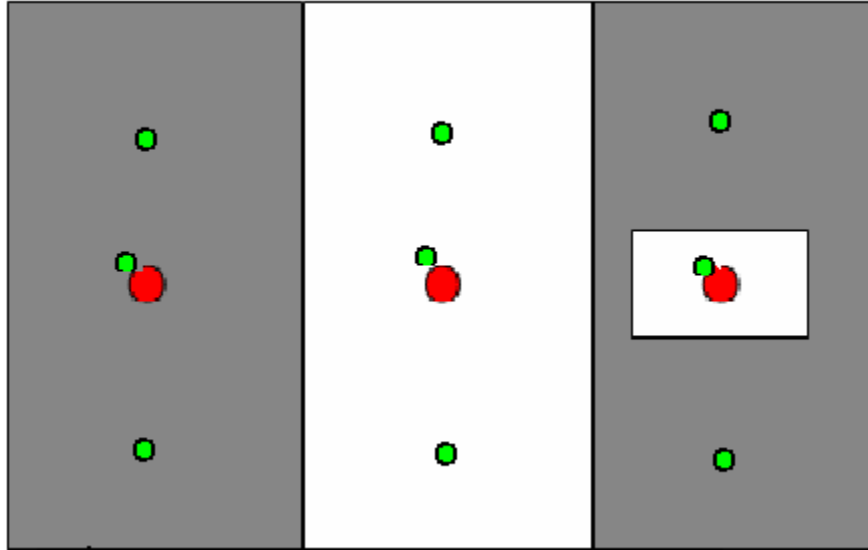
Fig. 19. Illumination pattern for lifetime test. Luminosity measurements taken at red dots.

The three different illumination zones were used to create areas of varying luminous flux and steady state temperature. The border between each zone was located on the boundary between two graphite heat spreaders in an attempt to minimize conduction between zones. A grid of nine thermocouples, shown as green dots in Fig. 19, recorded the screen temperature at different locations throughout the 1750 hour period. Luminosity measurements were taken every hour at the red locations in Fig. 19. A weekly luminosity "map" of the PDP was also generated in order to determine the luminosity profile of the entire screen. Since the CA-210 color analyzer only measures the luminosity at one point, a grid of 180 individual measurements was stitched together to create the map.

Temperature-Luminosity Dependence Test

The color analyzer was used in conjunction with the heaters to determine the effect of temperature on luminosity. Once steady-state conditions were achieved, the

temperature in a portion of the screen was elevated using the heaters. The luminosity was recorded every 30 seconds in both the elevated and un-elevated areas as the temperature rose towards the new steady-state condition.

Luminosity-Screen Loading Dependence Test

Measurements of luminosity variation with screen loading were performed. Luminosity measurements were taken at the center point of the screen after steady-state conditions had been reached.

Image Persistence Test

Finally, the color analyzer was employed to investigate the effect of the graphite heat spreader on image persistence. Both bright and dark image persistence was assessed using the illumination patterns shown in Fig. 20. First, an all-black image was applied to the screen for 60 minutes to suppress any previous image persistence. The 10-percent screen loading pattern was then displayed for 20 minutes, after which a full-white or full-black image was again displayed, depending on the type of image persistence being examined. Temperature and luminosity measurements were taken every minute at the screen center for 3.5 hours.

(Bright image persistence test) (Dark image persistence test)

(1)

(2)

(3)

"Ghost" persisting images
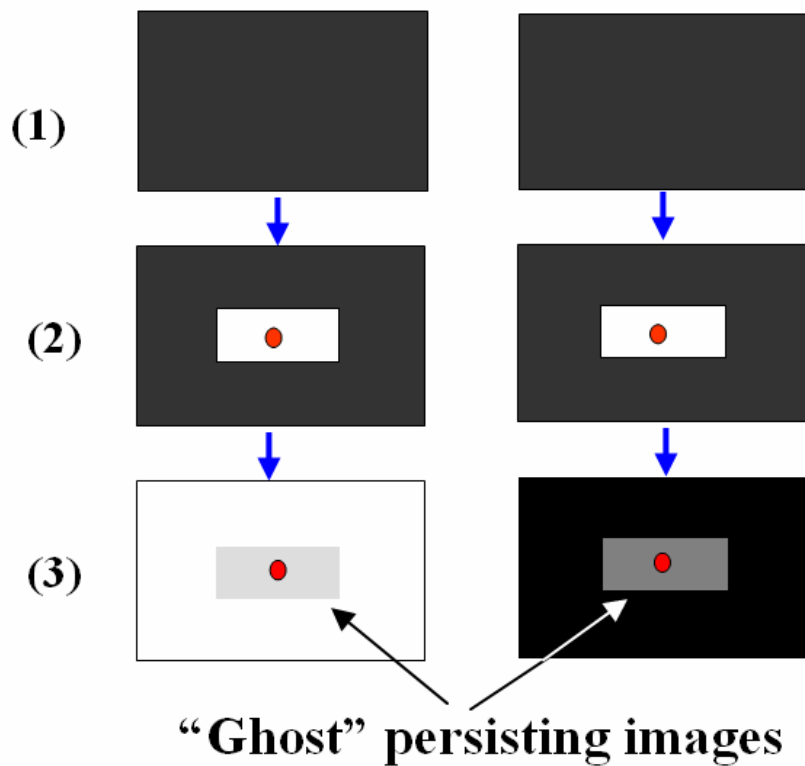
Fig. 20. Illumination pattern for image persistence tests. Luminosity measurements taken red regions.

Numerical Model

A three-dimensional numerical model of the PDP was created with Fluent 6.2 (Fluent, Inc.–Lebanon, NH) to predict the on-screen temperature distributions under various PDP operating conditions and to assess the effects of the anisotropic graphite heat spreaders. Fluent is a computations fluid dynamics (CFD) software package used to simulate fluid flow and heat transfer in complex geometries. Fluent provides complete mesh flexibility, solving flow problems with unstructured meshes that can be generated about complex geometries with relative ease. It uses the finite-volume method to solve the governing equations and provides the capability to use different

physical models, such as incompressible or compressible, inviscid or viscous, and laminar or turbulent flow. It can also solve the temperature fields generated by conduction, convection, and/or radiation heat transfer [25].
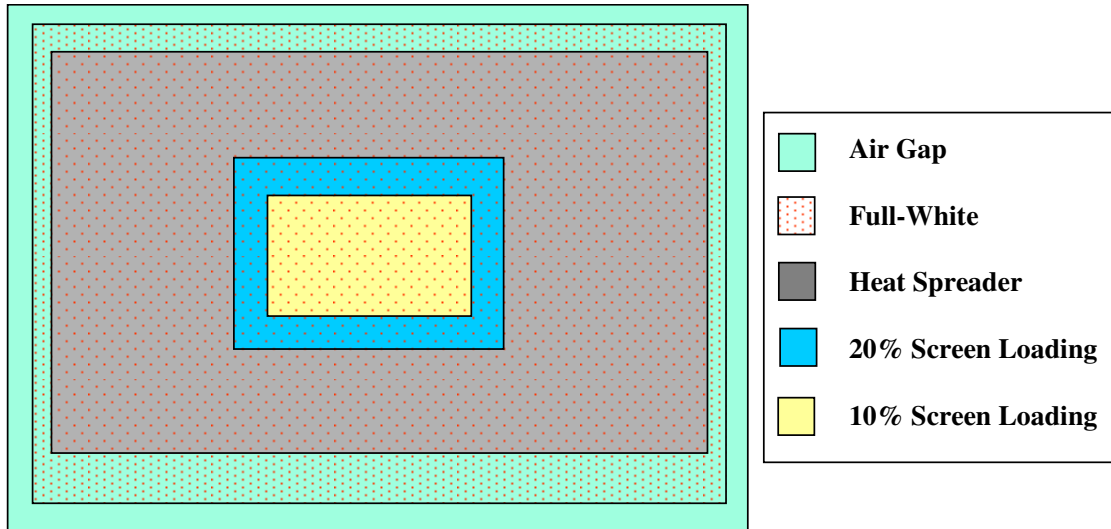
Fig. 21. Front view of numerical PDP model [24]
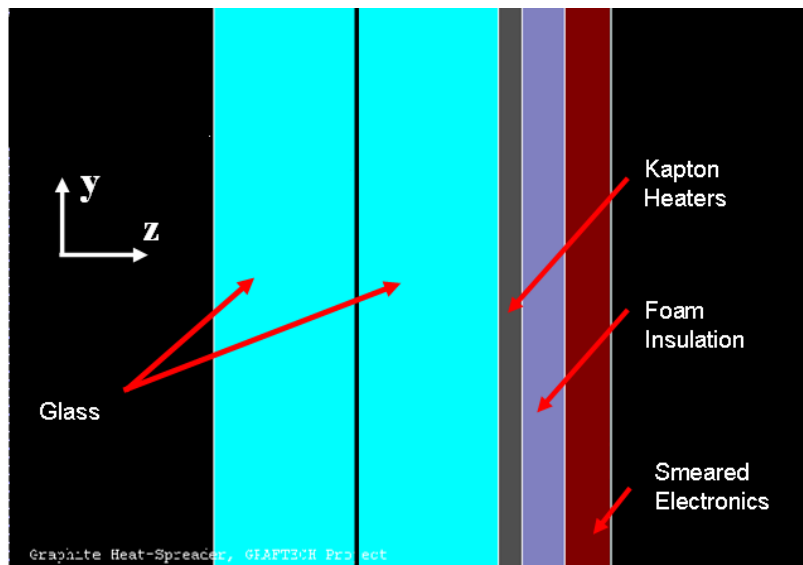
Fig. 22. Side view of numerical PDP model (not to scale)[24]

Fig. 21 and Fig. 22 show the model geometry used in the numerical simulation. Discretization of the PDP required that the model be separated into several regions and that roughly 25,000 hexahedron computational cells are used. The dimensions of the geometric features are summarized in Table 5.

Component	Dimensions W × H × t (mm)
Glass (2 layers)	$960 \times 580 \times 3$
Kapton Heaters	930 mm × 530 mm × 0.01mm
Foam Insulation	$960 \times 580 \times 3.175$
Aluminum Chassis	$960 \times 580 \times 2.2$

Table 5. Geometrical dimensions of the computational model components

In an operating PDP, heat is generated within two regions: the plasma cells and the control electronics. For the purposes of this study, the heat generated by the control electronics was assumed to be uniformly distributed across the chassis. Heat generated by the plasma cells was modeled as volumetric heat generation within a thin (0.1mm) layer in the center of the glass. The heaters, which were installed to provide control over the heat generation rate in the screen and simulating heat generation within the plasma cells, were modeled as a constant heat generation source on the back side of the glass. The layer of foam insulation between the heaters and the aluminum chassis was also modeled. A finite contact resistance was assumed to exist between the foam insulation and the aluminum chassis.

A convective boundary condition was applied on the front of the PDP. The external natural convection heat transfer coefficients on the PDP screen was determined from the commonly-used vertical flat plate correlation [26]:

$$\frac{\overline{h}L}{k} = \left\{ 0.825 + \frac{0.387 Ra_L^{1/6}}{\left[1 + (0.492/\text{Pr})^{9/16} \right]^{8/27}} \right\}^2$$

In this model, two different heat transfer coefficients were applied to the screen – one over the illuminated areas and a second over the unilluminated areas – and each was based on the average temperature taken through a vertical centerline in each area, yielding values typically between 3–4 W/m²K. Heat loss from the front of the screen due to radiation to the ambient was computed at each surface element by Fluent. The exterior edges of the chassis were treated as insulated boundaries, reflecting the modest temperature rise above ambient and their relatively small area.

A second convective boundary condition with an effective heat transfer coefficient representing both convective and radiative losses, in the range of 10 W/m²K, was applied to the back of the PDP. Uniform volumetric heat generation was assumed in the chassis. These assumptions proved to be acceptable in creating a first-order model of a PDP to predict on-screen temperature profiles.

In order to allow accurate temperature profile predictions, a thorough calibration of the numerical model with the experimental results was necessary. The following assumptions were used in this process:

- The heat transfer coefficient on the front can be calculated with the vertical flat-plate correlations using the average vertical temperature,

- The heat transfer coefficient on the back of the electronic chassis is constant,

- The heat flux in the screen is equal to the input power of heaters,

- A unique contact resistance, due to the application process and the thickness of heaters/insulation, exists for each spreader.

Based on these assumptions, the numerical model was calibrated with the experimental results by varying the contact resistance and heat transfer coefficient on the rear of the control electronics. This calibration process yielded contact resistance and heat transfer coefficient values of 0.016 K/W and 10 W/m²K, respectively, for the applied heaters—values that are quite reasonable considering the average screen temperature and the ambient temperature.

Experimental Results

Introduction

Experimental results for tests investigating the power consumption tendencies of the PDP, the effect of the heat spreader on temperature and luminosity, image persistence, the heaters, the temperature–luminosity relationship, and temporal effects on performance are discussed below.

PDP Power Consumption

The total input power to the plasma display unit, under different screen loadings and brightness settings, was measured using a power meter. The resulting values are presented in Fig. 23, showing the variation of PDP power dissipation across these two variables. In all the subsequent temperature mapping experiments reported herein, the brightness setting was kept to its original factory setting (i.e. 50%).
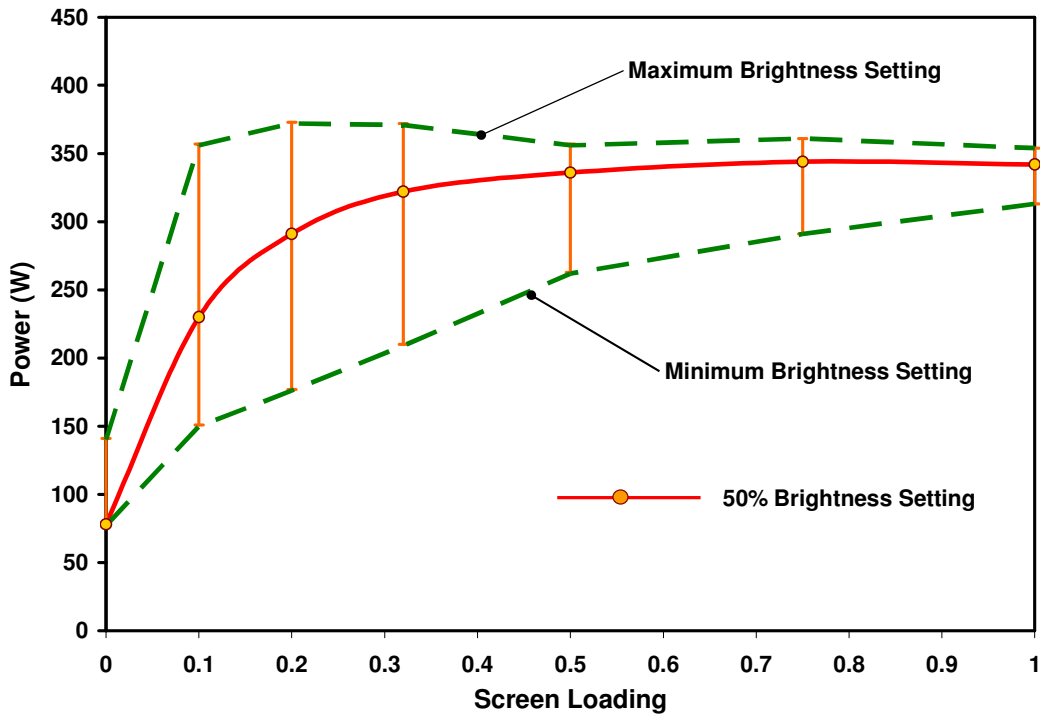
Fig. 23. Input power versus screen loading [23]

In Fig. 23, it can be seen that the power dissipation increases with screen loading, as the number of active pixels increases. However, the rate of increase of the power required to maintain the 50% brightness setting slows markedly beyond 50% screen loading and asymptotically approaches the power limit of 345W at a fully illuminated screen, i.e. screen loading equal to unity [23].

It appears that this behavior in the subject PDP can be attributed to the power control/management system which—beyond approximately 20% screen loading—moderates the total power consumption in the PDP by decreasing the luminosity of each active pixel as the number of illuminated pixels grows. The measured luminosity values, presented in Fig. 29, confirm this relationship. Interestingly, the instantaneous power measurement results, for a movie played on the PDP screen,

46

presented in Fig. 24, appear to suggest that approximately 20% screen loadings may

be typical for common video displays [23].
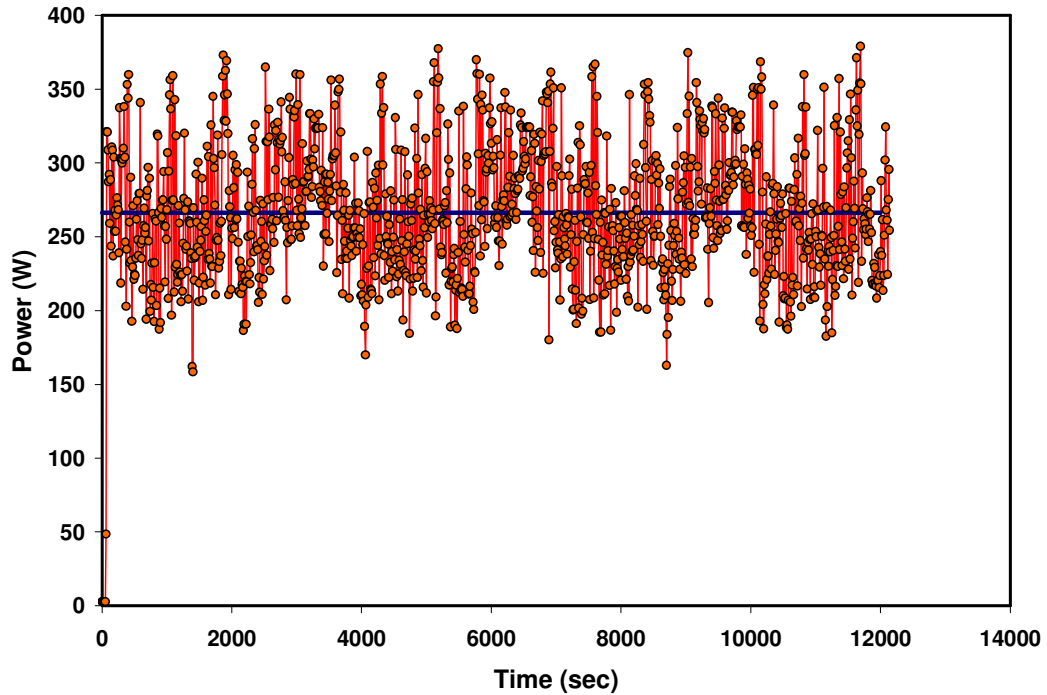
Fig. 24. Instantaneous input power to the PDP unit for an arbitrary movie [23]

As seen in Fig. 24, the average power consumption for this movie was

approximately 266 W, with a standard deviation of 47 W. Returning to Fig. 23, it can

be concluded that for this case the average screen loading is about 0.16 with a

standard deviation of 0.08 [23].

This conclusion assumes that – at the same screen loading - there is no

difference, in terms of power consumption, between the display of stationary images

and "motion pictures." This relationship is confirmed in Fig. 25, showing that the

power consumption of a stationary illuminated square in the corner of the screen was

identical to that of the same square meandering randomly across the full PDP screen.

Therefore, to allow for consistency and repeatability of the experimental conditions, subsequent tests of an operating PDP relied on the use of the 10%, 20%, and 100% illumination patterns [23].
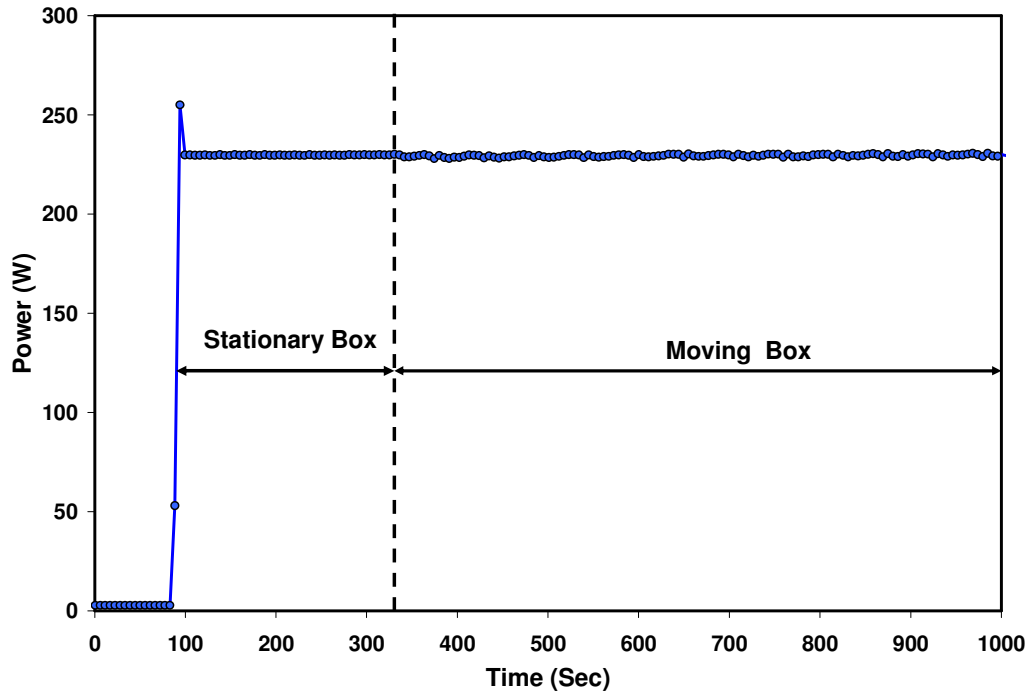
Fig. 25. Comparison between power consumption of motion and stationary pictures

It should be noted that the power dissipated in the screen cannot be explicitly measured because the ribbon cables connecting the control electronics to the plasma cells do not facilitate accurate determination of the power supplied to the screen. Moreover, the investigator's inability to control or modify the PDP's power management algorithm made it impossible to systematically vary the heat generation in the screen. To more precisely quantify the heat generation in the screen, in support of the development and validation of the PDP thermal model, use was made of

electrical resistance heaters attached to the back of the PDP, as described in a subsequent section of the *Heater Array* chapter.

Heat Spreader Effect–Temperature Measurements Luminosity Measurements

A comparison between IR thermographs for the high and low conductance heat spreaders is displayed in Fig. 26 for three screen loadings. These experiments were conducted without the EMI shield. In this figure, the beneficial effect—a 12°C decrease in peak temperature at 20% screen loading—of the in-plane conductance increase on the maximum screen temperature can be clearly seen for the 10% and 20% screen loadings. However, for the fully loaded screen the heat spreader conductance does not significantly affect the screen temperature map. Note that the anticipated trends in the temperature distribution are clearly evident in Fig. 26. Increasing the spreader conductance decreases peak temperatures but increases the temperature in the sides of the screen due to conduction from the hot spot.

High Conductance Heat Spreader Low Conductance Heat Spreader

Screen Loading=10%

Screen Loading=20%
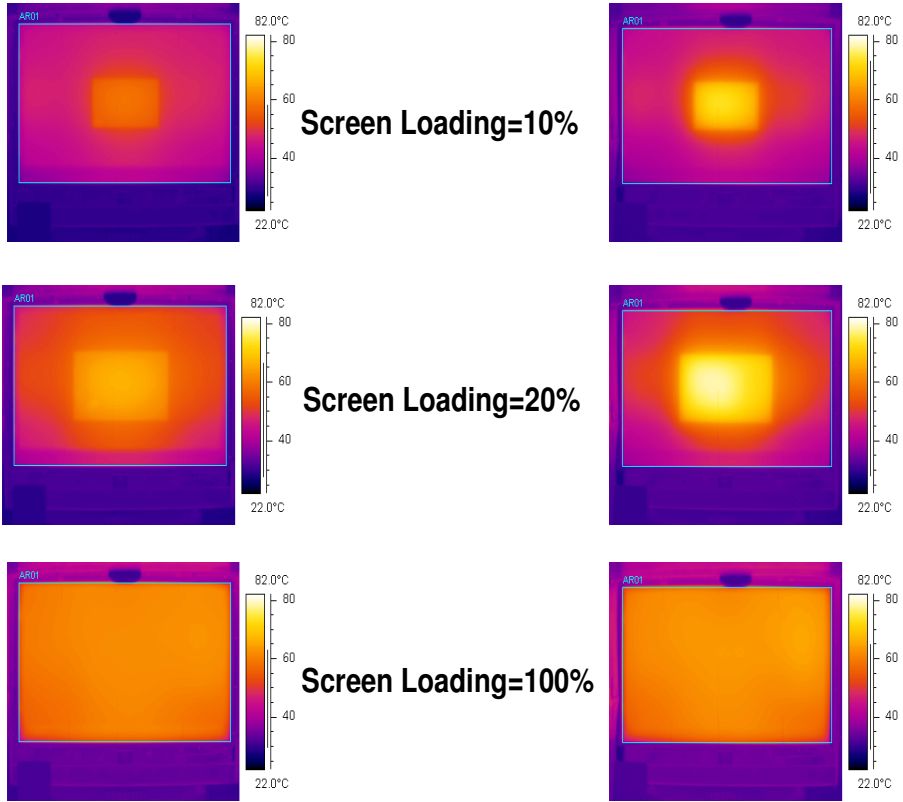
Screen Loading=100%

Fig. 26. Infrared thermographs of the PDP screen for high and low conductance heat spreaders [23]

In Fig. 27 the variation of the maximum and average excess temperatures of the screen versus the screen loading, for three different heat spreaders, is presented. Notice that the screen temperature increases to a maximum when the screen loading is about 20%. This temperature peak coincides to the maximum luminous flux generated by the PDP, which increases as the screen loading approaches 20%. Between 20% and 100% screen loadings, the luminosity decreases, as does the screen temperature. As seen in this figure, the maximum excess temperature (i.e. maximum screen temperature minus ambient temperature) for the low and high conductance cases can differ by more than 12 °C, or 25% of the excess temperature. Use of high

conductance graphite heat spreaders attached to the back of the plasma screen is thus seen to enhance lateral conduction of heat away from the relatively warmer white zones to the cooler zones of the PDP. However, the average excess temperature of the screen is not greatly affected by the heat spreader properties and can be primarily attributed to convective and radiative transport from the heated screen to the ambient air. It can be concluded that the in-plane heat spreader conductance plays a most important role in controlling the spatial temperature variation and peak excess screen temperature under this test scenario [23].

As previously noted, prior to the performance of the reported experiments, the EMI shield had been removed. However, using thermocouple measurements, it was found that the screen temperature can be 10 °C higher for the full white screen when the EMI shield was installed over the screen [23].
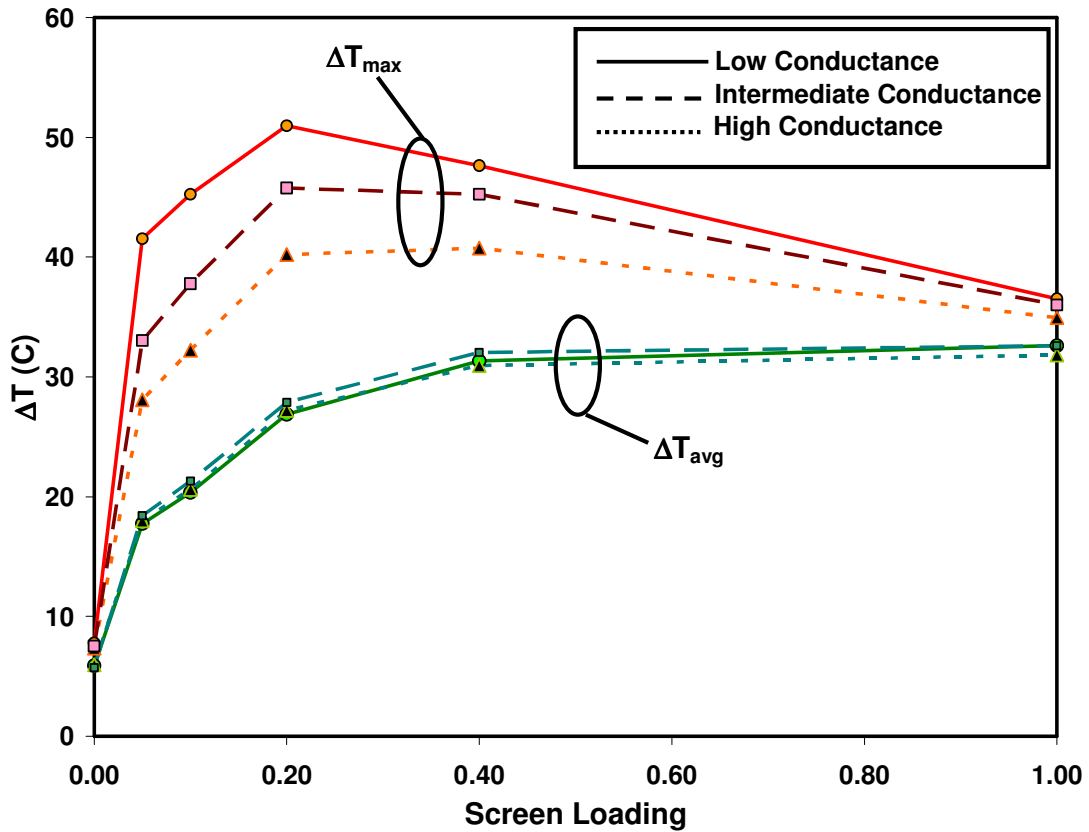
Fig. 27. Variation of maximum and average excess temperatures of the screen versus the screen loading [23]

While Fig. 27 highlighted the maximum temperature encountered on a PDP screen operated with a central intensely illuminated zone, Fig. 28 presents the variation of screen excess temperature along the horizontal centerline, as captured by the IR camera. The results clearly show the beneficial effect of the heat spreader when a non-uniform illumination pattern exists. However, for a full white or black screen, heat spreader conductance does not notably affect the temperature variation. It is believed that the observed asymmetry in the temperature profile with respect to the vertical centerline is due to greater heat generation by the control electronic components behind the right side of the screen. Despite this asymmetry, the expected

trends are still present—lower peak temperatures and higher edge temperatures as spreader conductance increases, for a constant screen loading. Also, the high conductance spreader has a noticeably steeper temperature gradient at the boundary of the illuminated area when compared to the low conductance spreader. This trend is also as expected due to the higher in-plane conductivity [23].
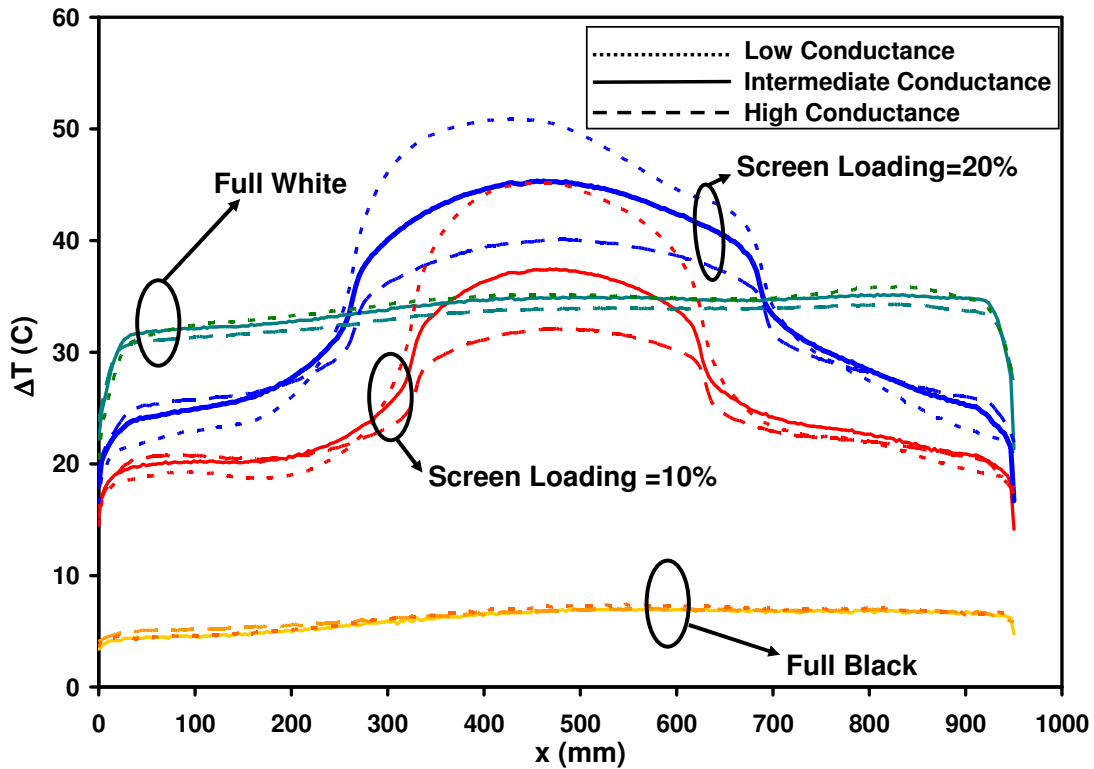
Fig. 28. Variation of the excess temperature along screen centerline for different heat spreaders and screen loadings [23]

Heat Spreader Effect–Luminosity Measurements

The variation of screen luminosity, measured at the center of the screen, with the screen loading is shown in Fig. 29. As seen in this figure, the increase in screen loading results in a reduction in the luminosity. A change from 10% to 20% screen loading results in approximately a 6.5% decrease in luminosity. The change from

20% to 100% screen loading results in a substantial 60% decrease in luminosity. This decrease is attributed to the power management system in the PDP that is modulating the brightness and power input to the screen. It is important to note that the human eye cannot discern a difference in brightness when the screen loading is changed, due to the lack of adjacent boundaries for comparison.

Additionally, increasing the spreader conductance results in a modest increase in luminosity at low screen loading values. Luminosity values with the high conductance spreader are roughly 5% and 4% higher than the low conductance spreader at 10% and 20% screen loadings, respectively. The spreader has no effect on luminosity at 100% screen loading. Although the reduction in temperature due to the spreader conductance is a likely cause for the luminosity increase, additional tests are needed to quantify this effect.
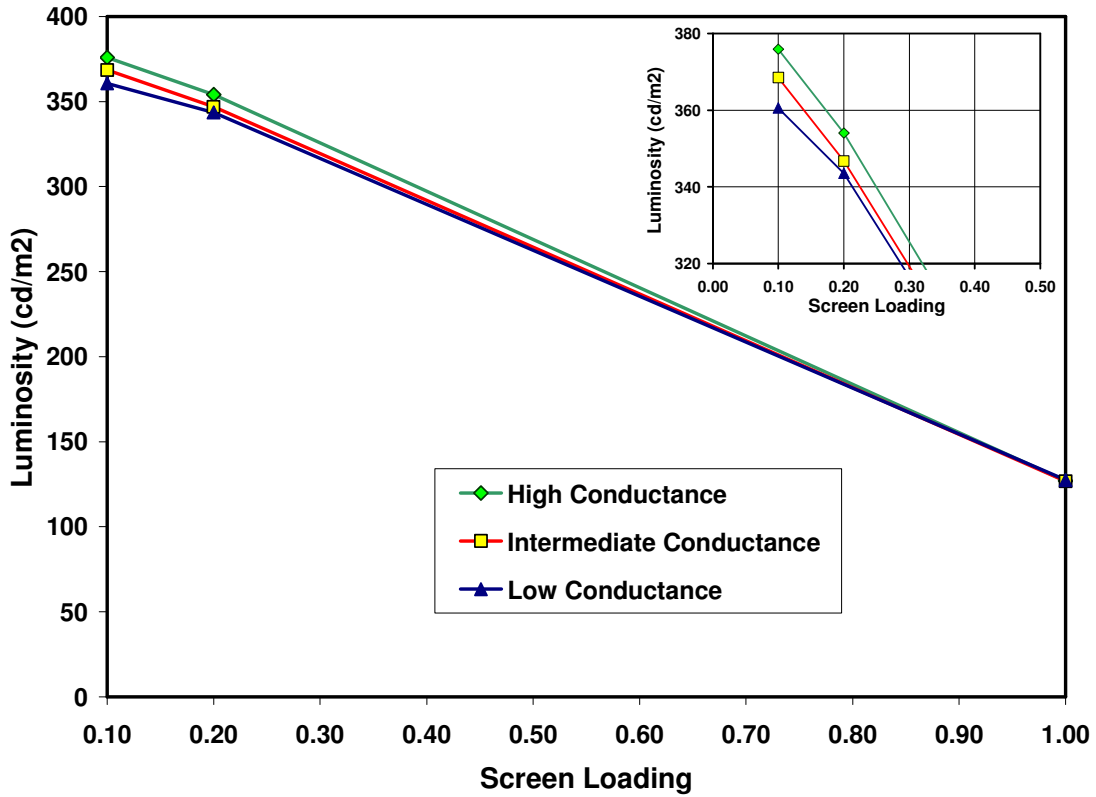
Fig. 29. Variation of luminosity with screen loading for different heat spreaders [23]

Image Persistence

The illumination patterns shown in Fig. 20 were generated using the VGA output from a laptop computer in order to quantify the effect of the heat spreader on the image persistence phenomenon, using the low and intermediate conductance spreaders. To analyze bright image persistence, the 10% screen loading image was displayed for 15 minutes, after which an all-white image was shown. The luminosity and temperature were measured for three hours at the center of the screen following the image switch to all-white. The bright image persistence results are shown in Fig. 30. Notice that the luminosity takes roughly 45 minutes to reach a steady state value. The luminosity tends to initially overshoot the steady state value and then decay to its

final value. As hypothesized in Tae, et. al., this trend may be related to temperature. Fig. 30 supports this, because the increase in luminosity is matched by a subsequent decrease in temperature. Although there is not a clear, evident difference in the persistence time between the two spreaders, it makes sense that the higher conductance spreader would have a slightly shorter total persistence time due to its lower conductive time constant. However, the luminosity response time of the PDP to changing temperatures is likely too slow to take advantage of this effect.

Fig. 30. Bright image persistence for low (k=140 W/mk) and intermediate (k=305 W/mk) conductance heat spreaders

Fig. 31 shows the dark image persistence results for the two spreaders. In this experiment, the 10% screen loading pattern was switched to an all-black screen, and the corresponding temperature and luminosity values measured. Tae, et. al. surmise that dark image persistence is due to an overactivation of the MgO layer and an

ensuing decrease in its secondary electron emission capability—a process that is not sensitive to temperature (at least in this range). The dark image sticking results show that both the low and intermediate conductance spreader cases take roughly 2.5 hours to reach a steady-state value. Temperature, on the other hand, reaches steady-state in about 45 minutes. As a result, it can be concluded that temperature, as well as spreader conductance, does not have an important effect on dark image sticking.

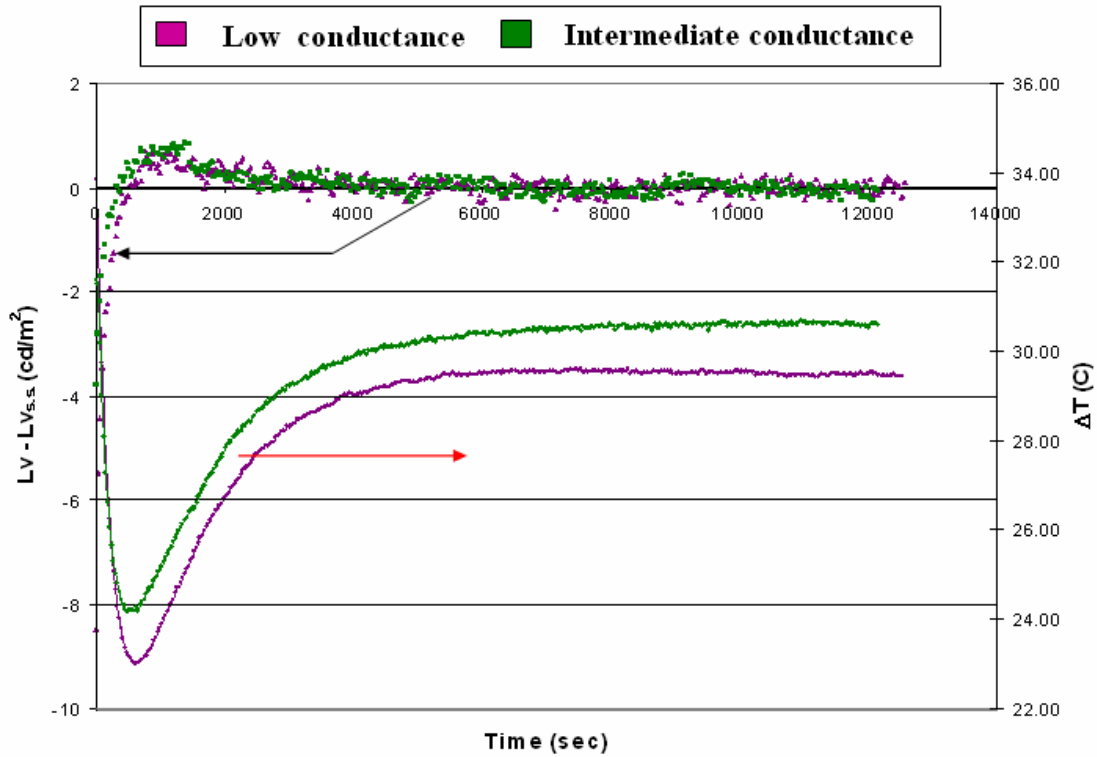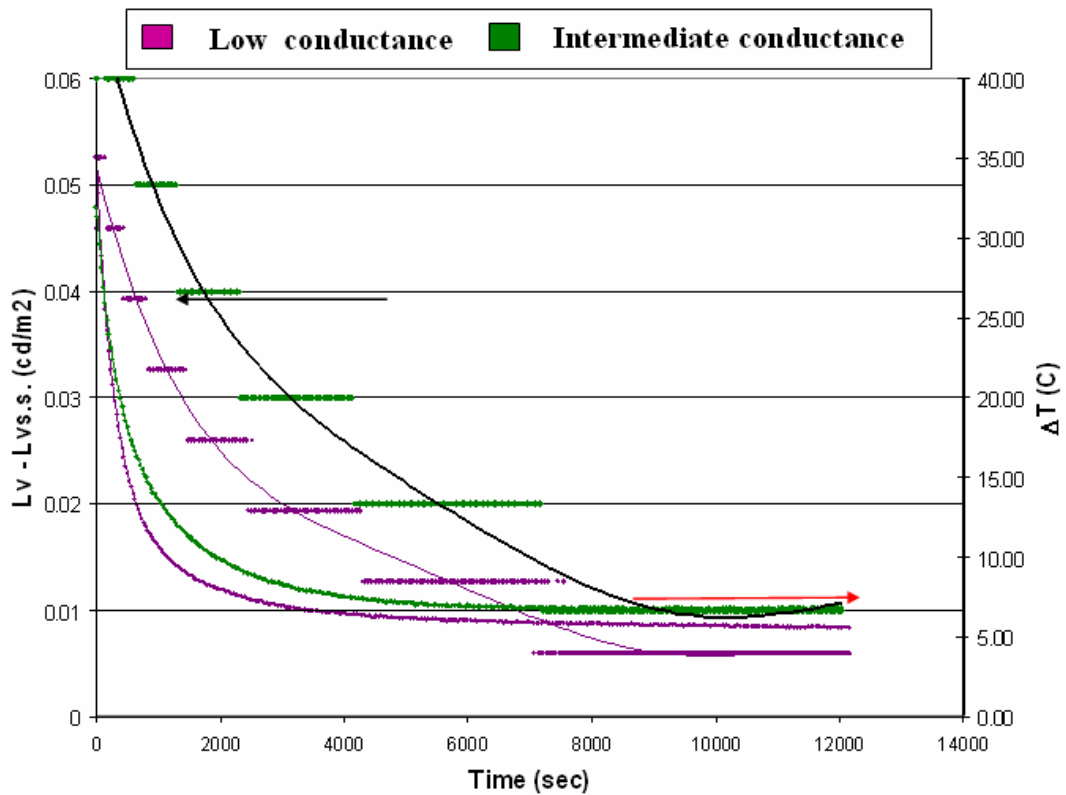*Fig. 31. Dark image persistence for low (k=140 W/mk) and intermediate (k=305 W/mk) conductance heat spreaders*

Note that the image persistence phenomenon, present in both Fig. 30 and Fig. 31, has only been shown in the center of a 10% white box that was rapidly switched to either an all-white or all-black screen. In the other regions of the screen that were

initially unilluminated, the change to all-black or all-white illumination was virtually instantaneous.

Heater Measurements

In these experiments, performed after electrical resistance heaters were attached to the back of the PDP screen, the power dissipated in the various parts of the PDP was determined through the readings on a digital multimeter attached to the heaters. These heaters were used to recreate the thermal map of the operating PDP, taken earlier at steady-state conditions for various screen loading values. It was then assumed that the energy dissipated in the plasma cells when the screen was operational was equal to the heater power, shown in Table 6. Since the input power to the PDP was known, the difference between the heater power and the total power was assumed to be dissipated in the control electronics. These values of power and heat flux are shown in Table 6.
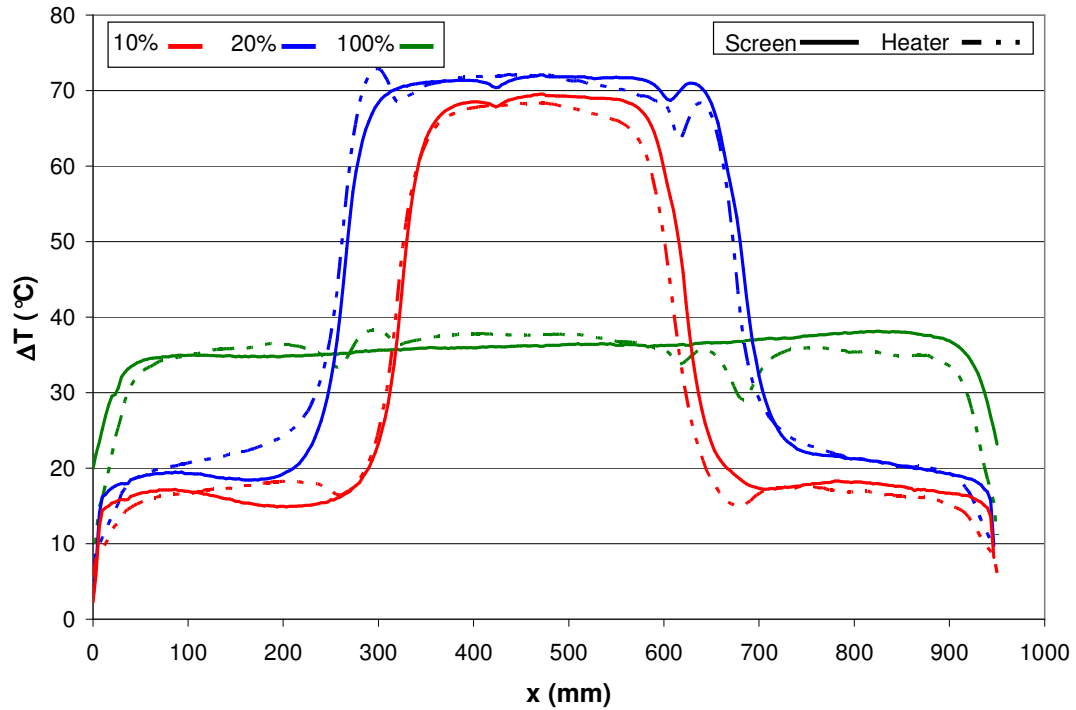
Fig. 32. Variation of the excess temperature along screen centerline for various screen loadings – intrinsic and extrinsic heating [24]

Screen Loading	Total Power	Power Dissipated in Active Area of Screen	Power Dissipated in Inactive Area of Screen	Power Dissipated in Electronics
10%	224 W	131 W	41 W	52 W
20%	308 W	222 W	54 W	32 W
100%	352 W	321 W	---	31 W

Table 6. Power allocation for various screen loading magnitudes

Fig. 32 presents the variation of screen excess temperature along the horizontal centerline, as captured by the IR camera, for both the heaters and the operational PDP. Note that for the input powers listed in Table 6, very good

59

agreement is seen in the "plateau" of high temperature associated with the brightly illuminated/heated zone between the two temperature profiles. Good agreement exists, with an average discrepancy of less than 3%, for the entire temperature profile for all three illumination patterns. It is nevertheless to be noted that Fig. 32 reveals a modest asymmetry in the temperature profile for all three intrinsically-heated PDP cases, with the left "side-lobe" of the screen temperature profile operating 1-2 K below the right "side-lobe." Interestingly, it is the right "side lobe" where the intrinsically and extrinsically-heated profiles agree best. This asymmetry may be due to the non-uniform distribution of heat generation in the electronic components mounted to the chassis, to non-uniformities associated with the power distribution buses on the PDP, or to some assembly related variations in the PDP screen.

Temperature–Luminosity Dependence

Fig. 33 shows the variation of luminosity with its local excess temperature. This test was performed by allowing the PDP to reach its steady-state temperature, and then increasing the temperature artificially with heaters. Luminosity was measured during the transient period when the on-screen temperature was increasing. For a comparison, luminosity was measured simultaneously in two locations: an unheated area and a heated area. This test was performed for several different brightness settings, and at several different screen locations, all yielding similar results. The same test performed at steady-state conditions yielded results with less than 0.1% discrepancy from the results presented. The transient results are shown due to the ease in producing a smooth luminosity vs. temperature curve [24].
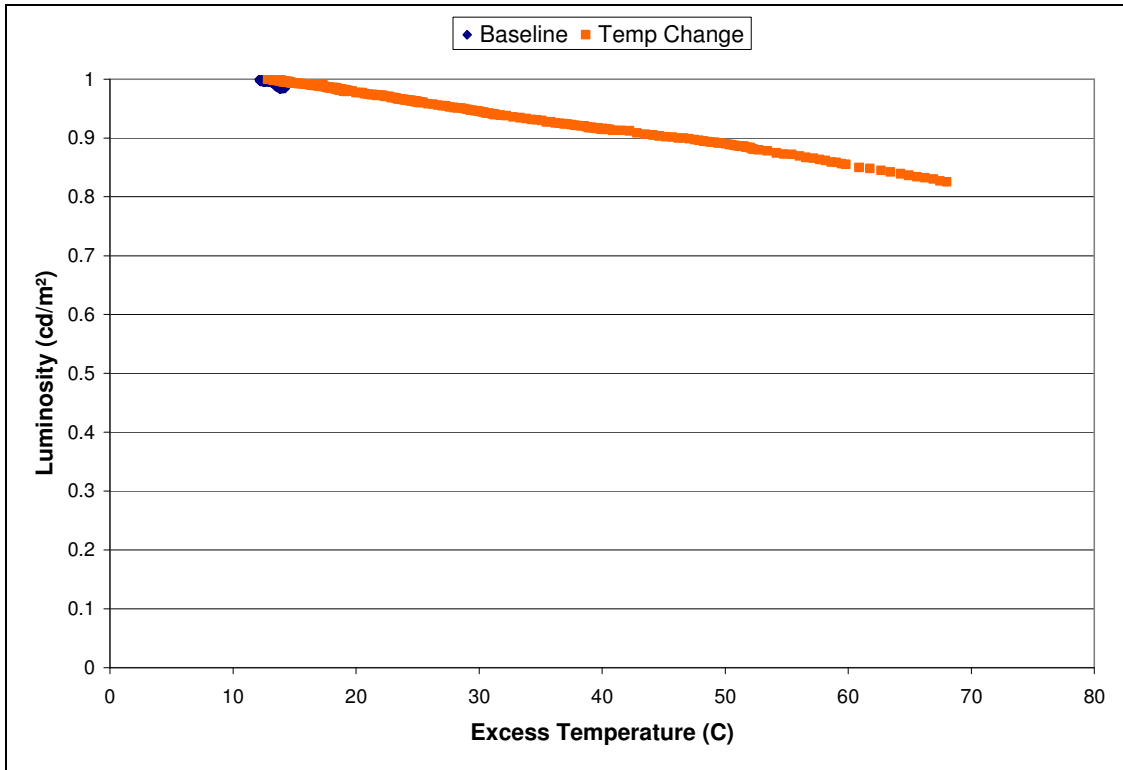
Fig. 33. Instantaneous luminosity vs. local excess temperature for artificially elevated screen temperatures [24]

The result clearly shows a linear correlation between luminosity and excess temperature, with approximately a 3.5 percent drop in luminosity for every 10 °C of temperature increase, or 0.11 cd/m²K. This confirms the expectation that an increase in screen temperature will result in a modest decrease in luminosity, and establishes the desirability of providing a means for reducing and/or controlling the maximum PDP screen temperatures.

Remember that the human eye is able to spot differences in luminosity of 0.8%. Theoretically, a 2.25K variation in temperature is enough to be noticed by the human eye; however, conditions that would allow the eye to spot these luminosity variations are not likely to occur. Even though the relative luminosity threshold is met, there usually is not a distinct boundary between the fully-luminous and the

degraded region. Instead, these boundaries are usually gradual, or obscured by more noticeable boundaries between unactive and active regions (such as the edge of a 10% or 20% box). One area where these distinct boundaries do occur is in cases of bright image sticking, and it seems that modulating the screen temperature to remove any temperature gradients would assist in reducing the persistence effect.

Lifetime Test

A full-screen luminosity map was taken of a brand new, stock PDP. The result is shown in Fig. 35a. Note that the as-received, unused PDP did not have a uniform brightness across the entire screen area. Natural variations of over 15% were present. Surprisingly, these variations were not noticeable, and the screen appeared to be uniformly white when entirely illuminated. This can only be attributed to the lack of distinct boundaries.

As previously described, hourly luminosity measurements were taken at the locations shown in Fig. 19, and comprehensive PDP screen mappings of luminosity were performed weekly. Measurements taken in the center of the white region and the box both showed roughly 15% decreases in luminosity over a 1750 hour period. This decrease is in the same range as that seen in literature—PDP manufacturer Planar reported 18% decreases in luminosity over a 1000 hour period for an all-white, statically illuminated screen. The slight rate difference is attributable to the design differences between brands in commercial PDPs. Not all screens are identical, and these results cannot be generalized to the entire PDP market. Still, decay rates were in the same range between the two screens [24].

The intent of various illumination zones was to create a range of luminous fluxes to quantify the effect of luminous intensity on screen degradation. However, the range of luminous intensity or differing steady-state temperatures was apparently insufficient to create a discernable difference in luminosity decay rates. Both the fully-illuminated area and the patterned area experienced similar decreases in luminosity. The all-black region experienced a much slower rate of luminosity decrease—this was expected due to the low flux in this area. These results are shown in Fig. 34.

Luminosity "maps" of the entire, fully-illuminated, PDP display surface were performed on a weekly basis. These maps, examples of which are shown in Fig. 35, consisted of 180 discrete measurement points in a uniform grid across the screen. A side-by-side comparison of the luminosity maps taken before and after the lifetime test show appreciable burn-in within the active areas. The natural variation in luminosity seen in the "before" image (Fig. 35a), was initially present in the PDP when it was first powered on. Fig. 35d, the "after" image, shows a larger range of luminosity and obvious burn-in effects. Fig. 35b and Fig. 35c show progressively worsening, permanent burn-in damage to the screen with increasing time of pattern display. The luminosity decreases were greater in the illuminated areas than in the un-illuminated areas, which is consistent with the results shown in Fig. 35. The result, displayed in Fig. 35, clearly shows a correlation between luminosity and the total time of PDP operation, with approximately a 12% decrease in luminosity over a 1750 hour period, or a luminosity deterioration rate of 0.02 cd/m²hr.
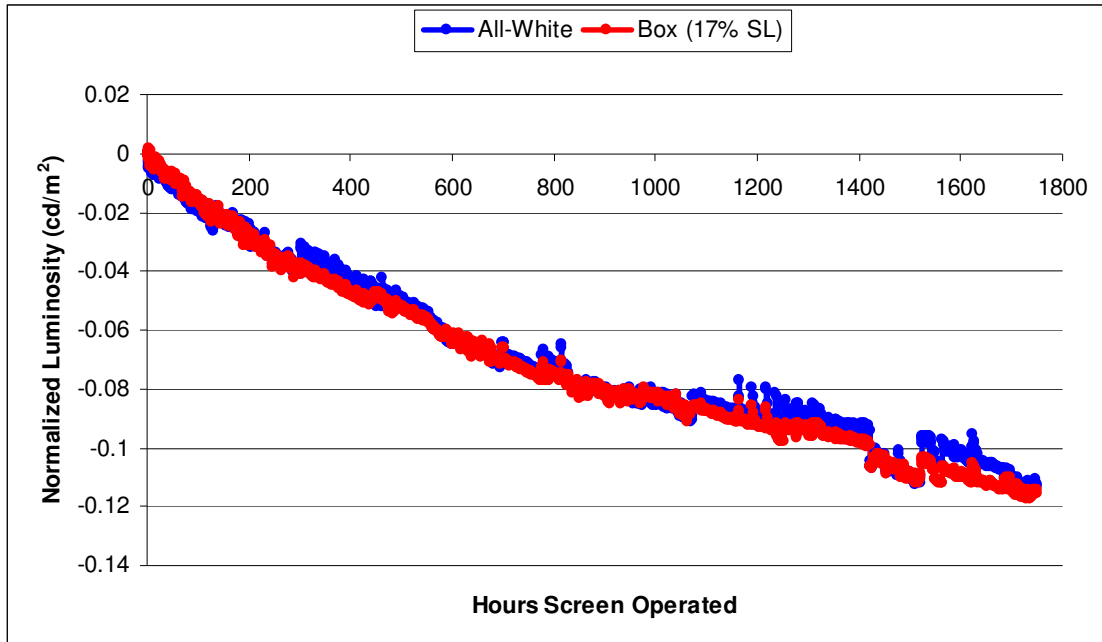
Fig. 34. Normalized luminosity decrease with time [24]

It is important to note that the natural variations in luminosity seen in the "before" image, of up to 25cd/m^2, were not evident to the human eye and appeared as a uniform white image. However, after 1750 hours, the so-called burn-in effects, representing a luminosity deficit of 32 cd/m^2, were easily noticeable to the human eye. Once again, this is due to the distinct boundaries between the illuminated and unilluminated zones, which were not present in the "before" image.

a)

b)
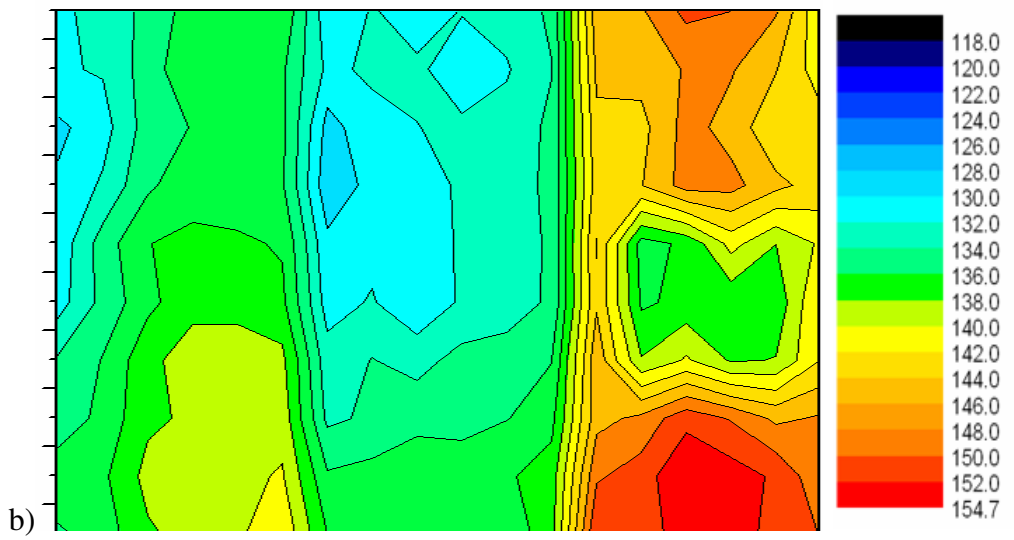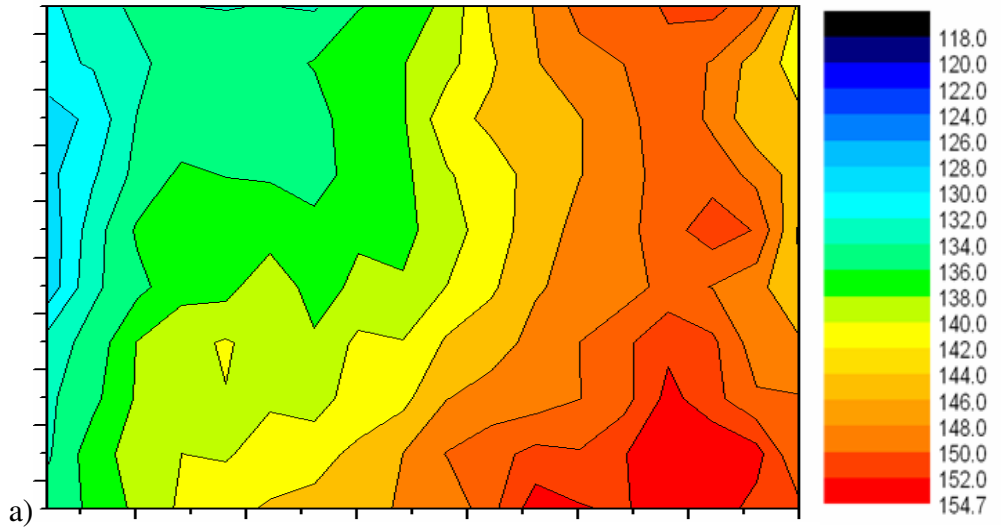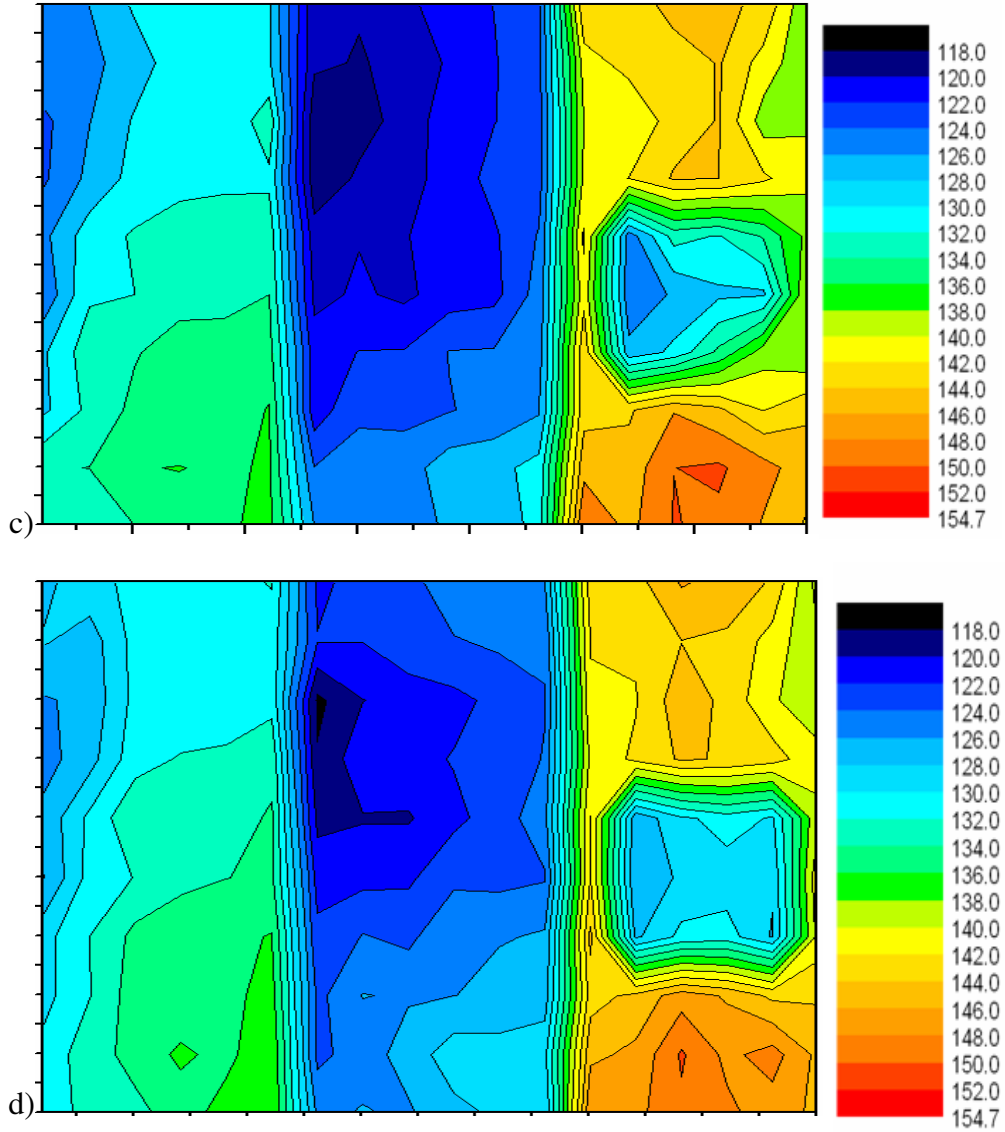
Fig. 35. Luminosity "maps" of PDP a) before life test, b) after 27 days, c) after 52 days, and d) after 73 days

Numerical Results and Discussion

Introduction

A three-dimension numerical thermo-fluid model was created to predict the temperature distribution occurring on a PDP for the previously tested display patterns. Since increasing temperatures have been proven detrimental to PDP performance, it is desirable to be able to predict on-screen temperatures, especially the peak temperature as this drives performance degradation, for various thermal management schemes. With an operational model, it is possible to optimize spreader geometry and conductance to best increase performance. Such tests would be very difficult to perform experimentally due to the intensive labor involved in removing and replacing the heat spreaders.

Comparison of Numerical and Experimental Results

The simulated temperature fields for 10 percent, 20 percent and 100 percent screen loading, respectively, are shown in Fig. 36. The model was calibrated according to the procedure outlined in the Numerical Model section above. Fig. 36 compares the actual PDP results, with heaters installed, to the numerical model results, also with the heaters modeled. The simulated values obtained with the calibrated numerical model closely agree with the empirical peak temperatures—the key thermal characteristic of the PDP screen—for differing screen loadings. These values also capture the spatial characteristics of the PDP temperature profile, namely the larger diameter hot spot for the 20% case, the slightly higher peak temperature in

the 20% case, and the slope of the temperature gradient at the edge of the hot spot [24].
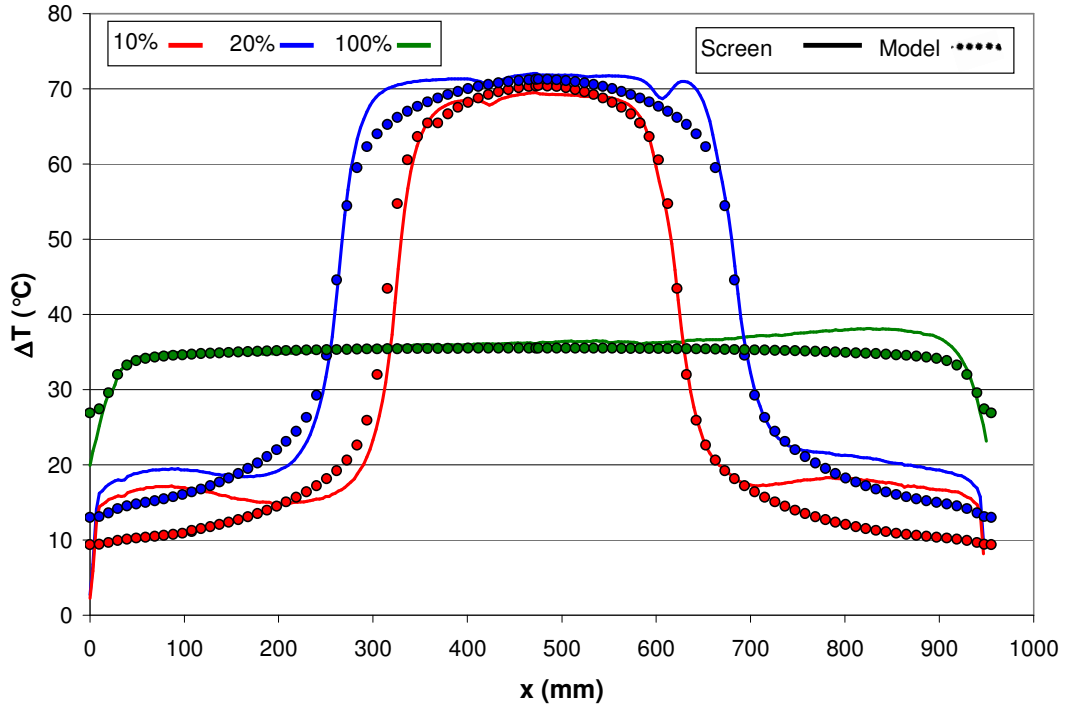
Fig. 36. Numerical and experimental variation of the excess temperature along the screen centerline for PDP with heaters, and no spreader, installed [24]

While the numerical thermal model displays the requisite ability to replicate the salient features of the PDP temperature field, to within typically ±1.5 K, it under predicts the screen temperatures in the unilluminated regions and fails to display the previously discussed, modest asymmetry visible in the experimental temperature profiles for the all-white screen. Interestingly, it appears that the numerically-predicted values are somewhat closer to the lower temperatures of the left side-lobe than the right, though better agreement is seen on the right upslope of the temperature profiles than on the left.
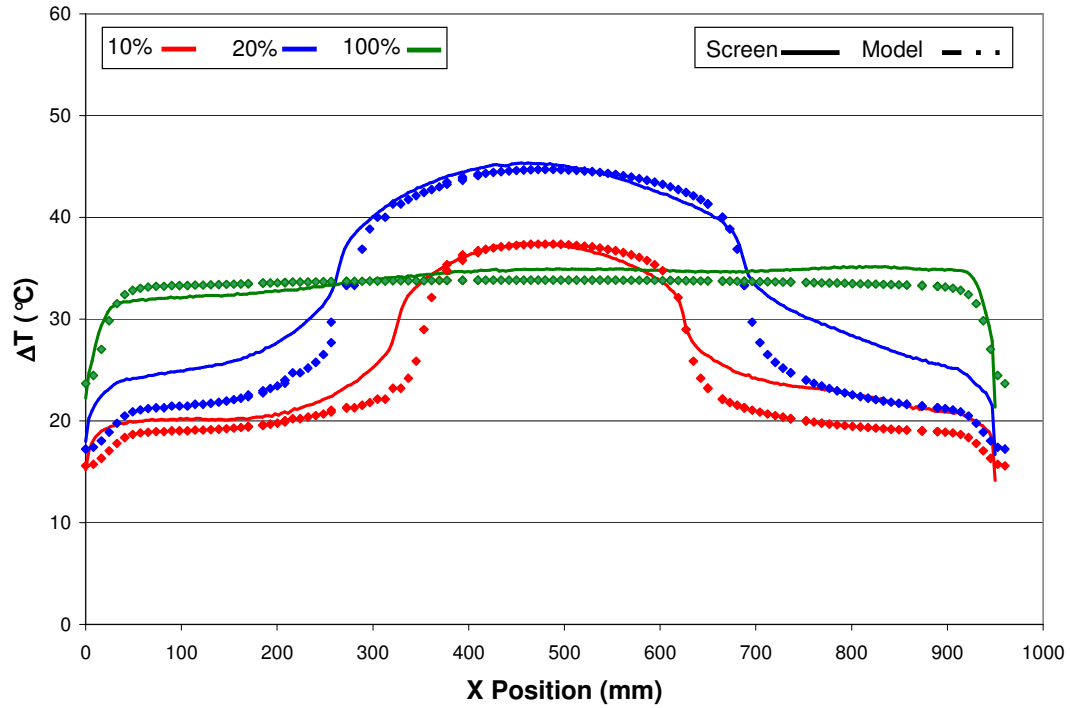
Fig. 37. Numerical and experimental variation of the excess temperature along screen centerline for intermediate conductance spreader[24]

The current thermo-fluid numerical model, carefully calibrated with the use of electrical resistance heaters, and modified to include the graphite heat spreaders described in Table 4, was used to generate PDP temperature profiles for the 10%, 20%, and all-white (100%) screen loading conditions. Fig. 37 demonstrates the ability of the numerical model to closely predict peak temperatures, and capture the spatial temperature variation near the center of the screen, for various screen loadings, when using the intermediate conductance heat spreader and a calibrated contact resistance value of 0.016 K/W. Once again, the model is unable to predict the side-lobe temperatures, and to reproduce the asymmetry present in the experimental results.

The effect of the heat spreader on the PDP temperature field is shown in Fig. 38, for steady-state conditions. The pattern resembles a "flattened" Gaussian distribution, with the peak temperature in the center amid a flat temperature plateau, and then steep decreases to flat "side lobes." A progressive reduction in the peak screen temperatures when moving from the thin, low lateral conductivity spreader to the thicker, higher conductivity spreaders is also clearly evident in this figure. It would appear that the lateral thermal conductance of the spreaders, i.e. the product of the in-plane thermal conductivity and the cross-sectional area, is the spreader property most responsible for this temperature reduction. The peak screen temperatures with the high conductance spreader are nearly 13K lower than the maximum temperatures with the lowest conductance spreader. Additionally, the edge temperatures outside of the illuminated zones are hotter with the high conductance spreader. This trend is consistent with expectations as the higher conductance spreaders enhance lateral conduction of heat away from the warmer white zones to the cooler zones of the PDP. However, the heat spreader does little to remove heat from the system, and as a result, the average temperatures are similar for each spreader case.
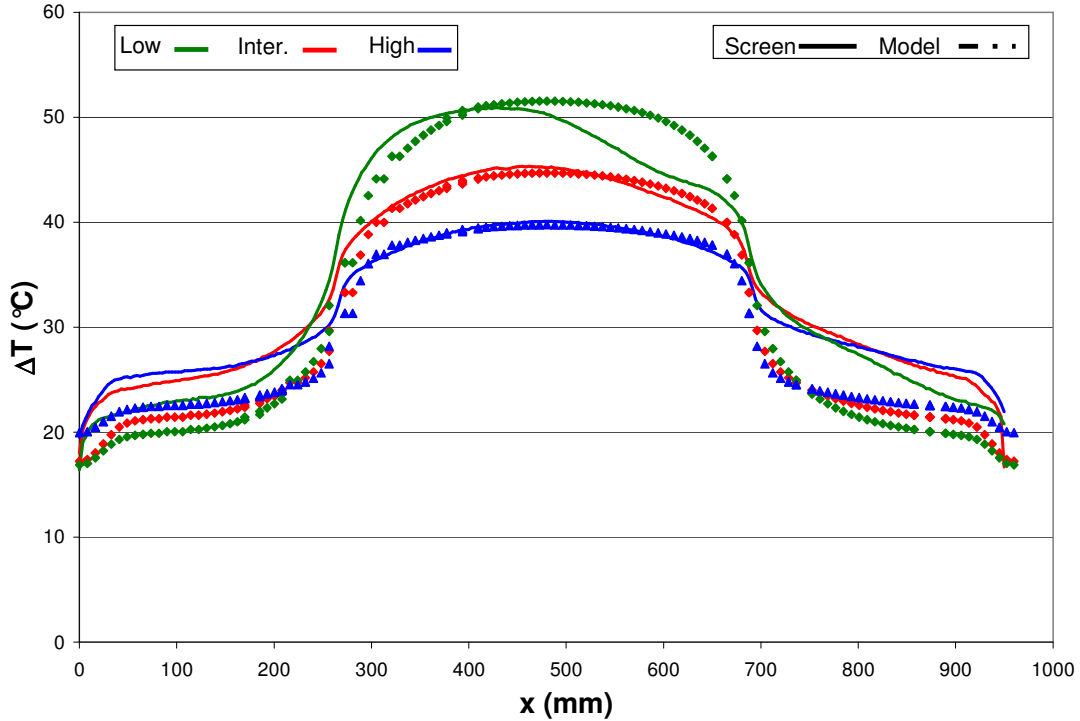
Fig. 38. Numerical and experimental variation of the excess temperature along screen centerline for low (k=140 W/mK), medium (k=305 W/mK), and high (k=440 W/mK) conductance spreaders at a constant 20 percent screen loading [24]

Using the validated numerical model, it is possible to study the impact of the geometry and properties of the heat spreader on the peak screen temperature and further explore the importance of the in-plane thermal conductance on the peak PDP temperature. Fig. 39 shows the variation of the predicted peak excess temperature with spreader conductance for several thicknesses and thermal conductivities in the range of: $0 \leq t \leq 1.4$ mm, 0.026 W/mK $\leq k_{xx} \leq 440$ W/m.K, and $.026$ W/mK $\leq k_{zz} \leq 10$ W/mK, along with the experimentally determined peak excess temperatures for the three spreader configurations at 10% and 20% screen loadings. To a first approximation, the excess peak temperature is well correlated with the in-plane conductance, but it requires slightly separate functions to describe the 10% and 20%

screen loadings: the 20% case is described by ΔT_{max}=-4.6 x ln(conductance) + 39.0, while the 10% case is described by ΔT_{max}=-4.9 x ln(conductance) + 29.8. Note that there is a natural-log dependence in both cases.

It is important to note that both curves can closely predict the six experimental points, representing the three spreader conductances at two different screen loadings. Next, it is evident that spreader conductance does have a large effect on peak temperatures when the curve is completed numerically, dropping from an excess temperature of 118K with no spreader to 39K with a spreader conductance of 0.66W/K. However, excess temperatures in the range of 118K will not occur experimentally, due to the in-plane conductance, and resulting spreading effect, of the glass. Compared to the conductance of the spreader, the glass will not have an appreciable effect on reducing peak temperatures. In the no-spreader case, the glass becomes very significant as the conductivity of the glass is 50 times that of air. Experimental results for the no-spreader case, shown as "Exp.-Insulation" in Fig. 39, depict maximum excess temperatures of 72.5K.

This excess temperature can be reduced to approximately 39K for 10% screen loading, and expected local luminosity increased by some 11%, with the use of a natural graphite heat spreader with a lateral thermal conductance of 0.66 W/K. Use of a far poorer conductance spreader, at approximately 0.07 W/K, results in a peak excess temperature of approximately 52K, and a somewhat diminished expected benefit in luminosity of 7%. Note that the beneficial effect of increasing conductance begins to weaken beyond values of approximately 0.25 W/K. Additional factors, such as the thru-plane spreader conductivity and the size of the air gap behind the

heat spreader, have been found to more weakly influence the screen excess temperature, due to the small temperature gradient (~75 K/m) through the thickness of the PDP.
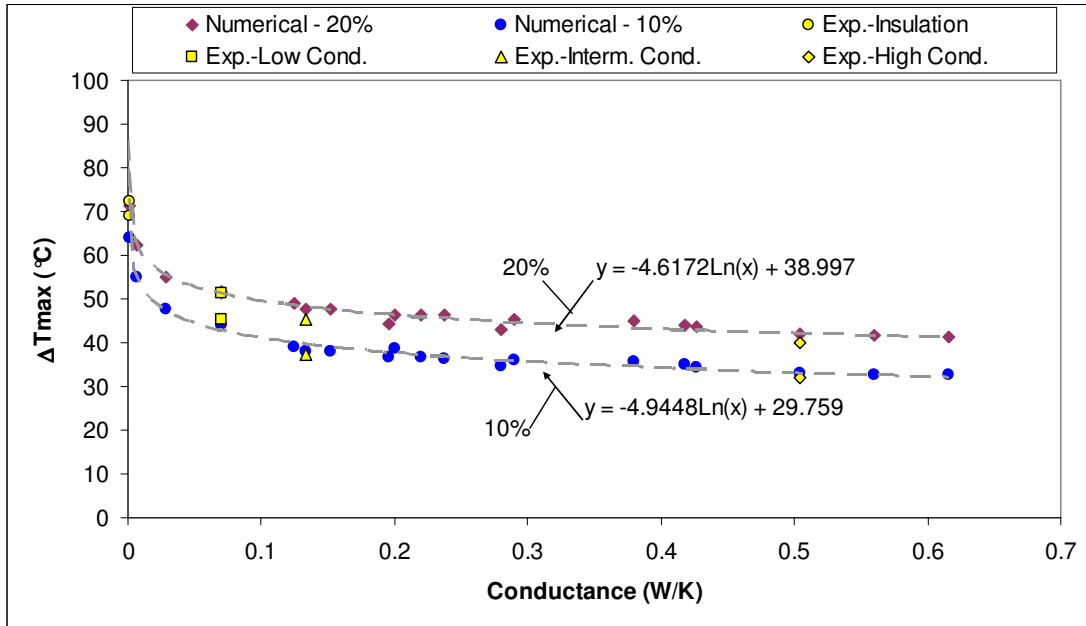
Fig. 39. Peak Excess Temperature for varying in-plane conductance at 10% and 20% screen loadings [24]

Numerical Results with Alternate Screen Patterns

Previous numerical simulations were confined to 10%, 20%, and 100% screen loading patterns. In order to determine the general utility of the numerical model and its applicability to the prediction of the PDP temperature distributions for other illumination patterns, the "donut" heating pattern shown in Fig. 40—with a dark area in the center, dissipating 21W, and a wide ring of illumination, dissipating 261W, on the remaining screen area— was applied to the PDP. To avoid the uncertainty associated with intrinsic heat generation in the PDP screen, attention was limited to patterns that could be generated with the attached heaters. The absence of heating in

73

the center of the PDP and a ring of heat generation around the periphery poses a severe challenge to the thermal model, calibrated with the inverse heating pattern (Fig. 36).
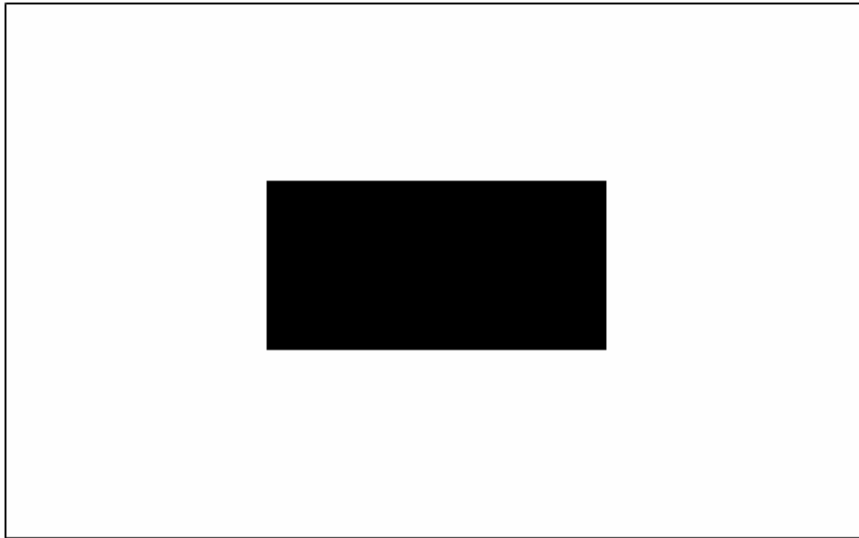
Fig. 40. Alternate PDP illumination pattern with 90% screen loading. Heat is generated in the white, or active, regions of the image.

The numerical and experimental results for this illumination pattern are shown in Fig. 41. Although the numerical model was not calibrated to predict this screen pattern, it was able to predict the center screen temperature within one degree, and the edge temperatures within three degrees. Previously, the model was proven able to predict the peak temperatures in the 10%, 20%, and 100% illumination patterns; however, these peak temperatures were also located in the center of the screen, and the model was unable to accurately predict the edge temperatures.
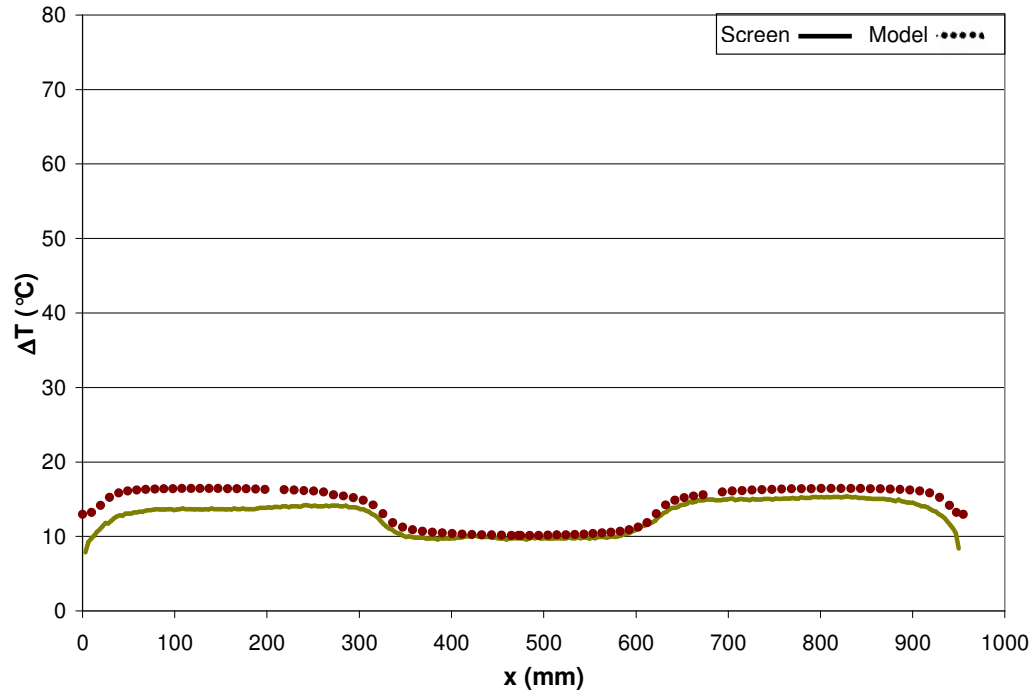
Fig. 41. Numerical and experimental variation of the excess temperature along screen centerline for 90% screen loading

The temperature profile comparison shown in Fig. 41 for the "donut" screen heating pattern highlights a discrepancy in both the temperature gradient and the temperature at the far edge of the screen. The experimental results contain a much steeper temperature gradient at the extreme screen edge than the numerical model predicts. This discrepancy may be due to either an inconsistency in the thermal/structural representation of the edge region of the PDP or a measurement error.

First, the model treats the screen edges as insulated boundaries. In reality, the PDP screen edge is surrounded by an aluminum chassis edge. In developing the PDP thermal model, it was expected that the chassis edge would not significantly contribute to the heat transfer from the screen because the total edge area is small compared to the screen area. Additionally, on one side of the glass an air gap exists

between the two surfaces, the other side is insulated by foam tape, and the spreader stopped short of the chassis—all contributing, it was thought—to a relatively high thermal resistance at this surface.

The experimental temperature contours illustrate that heat is flowing from the edge of the glass with a temperature gradient of approximately 225 °C/m. A first-order analysis of the heat loss from chassis edge due to convection and radiation to the ambient yields a theoretical heat flux of approximately 1100 W/m² from the edge of the PDP that could induce a temperature gradient of approximately 800 °C/m in the last few centimeters of the PDP. It is, thus, understandable that with some "contact" resistance at the edge, the heat loss and hence the temperature gradient at the edge of the PDP is only a fraction of this theoretical value.

It is also possible that the infrared measurements of the PDP temperature profile are compromised by the limited spatial resolution of the IR camera, estimated at 4mm-5mm, and the effect of the strong emissivity difference between the nearly-black (radiationally) glass panels of the screen and the low emissivity polished aluminum chassis. In determining the overall temperature distribution of the meter-long PDP, these two effects can be expected to be negligible. However, the comparatively low emissivity of the chassis, which was not corrected in the IR imaging study, could induce an error of several degrees in temperature and contribute to an unnaturally steep temperature gradient at the extreme edge of the PDP.

The above considerations suggest that a higher fidelity numerical model would require additional attention to the boundary conditions imposed on the PDP edge. An analytically or an experimentally-determined heat flux or temperature

gradient should be applied as the boundary condition. Alternatively, the numerical model could be expanded to include the PDP frame which could then be allowed to convectively and radiatively exchange heat with its surroundings. Since the goal of this modeling study was to predict the peak temperature of an interior area of the PDP screen, and more particularly a centrally located hotspot, the edge region did not receive extensive attention. This goal was successfully accomplished with the thermal model developed in this study, but the proposed enhancements could be expected to extend the accuracy of the numerical model to the entire PDP area.

Conclusions for Numerical Results

In summary, a numerical model has been created that can predict peak temperatures, within 1.5K, of a PDP with centrally-located illuminated regions for various in-plane conductance natural-graphite heat spreaders. Numerical predictions for spreaders of very low conductance show very high peak temperatures, implying that almost any spreader is better than no spreader. However, peak temperatures can continue to be effectively reduced by increasing spreader conductance up to about 0.25 W/K.

Although the numerical model was able to reproduce the salient features of the PDP temperature distribution, it did fall short in several areas. First, the model was unable to match the temperature gradient at the edge of the screen. This is most likely do the fact that the model treated the edges like insulated boundaries, while in reality they are not, and possible measurement errors near the aluminum chassis.

Second, the model fails to match the asymmetry seen in the experimental results. This is most likely due to non-uniformities in the electronic heat generation,

which was assumed to be uniform in the numerical model. Future models could more accurately address power dissipation in the electronics.

Finally, the model under-predicts temperatures in the side-lobe regions. This is possibly due to several reasons. The applied heat transfer coefficient in the side region might be artificially large. It is based on the average vertical temperature in the side-lobe; however, these correlations are not perfect and the applied heat transfer coefficient is only an approximation. An artificially large heat transfer coefficient would unnaturally decrease temperatures. Additionally, the electronic power dissipation in the chassis might be highly, yet non-uniformly, skewed to the edge regions of the screen. The applied uniform heating in the chassis may have compromised the accuracy of the less-important "side lobes."

This numerical thermo-fluid model was driven by a desire to fit the critical parameter—the peak temperature—at the center of the screen. Predicting the side temperatures or the temperature distribution of the electronics was not the aim of this model. Future models could be calibrated differently to produce more accurate renderings of the temperature profiles on the exterior regions of the screen. Despite the apparent shortcomings in this model, the beneficial effects of the natural graphite heat spreader have still been shown.

Conclusions

1. A laboratory PDP test apparatus, based on a commercial PDP and modified to include graphite heat spreaders and electric heaters, was constructed and used to determine the effect of spreaders on the PDP temperature distribution for an imposed illumination/heating pattern, as well as the spatial, temporal, and thermal variations of screen luminosity.

2. A thermal, finite volume, numerical model was successfully developed and calibrated with experimental results and used to broadly investigate parametric trends in the PDP temperature and luminosity fields, and to help optimize the dimensions and conductivities of the on-screen heat spreader.

3. The numerical model was shown to be capable of predicting the temperature distributions for a variety of illumination and heating patterns, achieving 1.5K accuracy in the most critical, peak excess temperature on the screen.

4. For the test illumination pattern and the PDP screen, a high in-plane conductance graphite thermal spreader was found to reduce peak screen excess temperatures by over 30K (>45%) when compared to the no-spreader case, and to reduce the severity of on-screen temperature gradients.

5. Numerical simulations reveal that an on-screen excess temperature as high as 72.5K can be expected to occur with a 20% illumination pattern and no heat spreader on the PDP screen.   This excess temperature can be reduced to approximately 40K, and expected local luminosity increased by some 11%, with the use of a natural graphite heat spreader with a lateral thermal conductance of 0.66 W/K. Use of a far poorer conductance spreader, at approximately 0.07W/K results in

a peak excess temperature of approximately 52K and a somewhat diminished expected benefit in luminosity of 7%.

6. The current research effort has shown that—for the test PDP screen—increasing screen temperature has a deleterious effect on screen luminosity, leading to a 3.5% reduction in luminosity for every 10K increase in screen temperature. Moreover, experimental measurements have revealed that the luminosity of the commercial PDP screen, operating at a constant temperature, decreased with operating time, falling 15% after 1750 hours of operation for the brightly illuminated sections of the PDP screen. These results suggest that a 2.25K change in screen temperature or roughly 50 hours of screen aging would be detectable by the human eye.

7. Experimental results reveal that reducing temperature has a modest effect on diminishing the severity of bright image persistence, but has no effect on dark image persistence. Consequently, increasing spreader conductance will assist to reduce bright image persistence, although the extent of the improvement is difficult to quantify because the human perception of image persistence is dependent on the exact image that is persisting and the presence of boundaries between areas of high and low luminosity.

Bibliography

[1]   Lee, M. and Pecht, M., "Thermal characteristics of glass-metal composition plasma display panels," *IEEE Transactions on Advanced Packaging*, vol. 25, pp. 488-494, 2002.

[2]   Bianco, C. "How Vision Works." [Online] Available: http://health.howstuffworks.com/eye.htm. September 6, 2006.

[3]   (2002). How Plasma Displays Work. HowStuffWorks. [Online]. Available: http://electronics.howstuffworks.com/plasma-display.htm

[4]   Bignon, T., Boher, P., Gibour, V., Leroux, T. "Image Sticking Cartography on PDP TV: A New Quantitative Measurement." SID Symposium Digest of Technical Papers. Volume 36, Issue 1, pp. 598-601, May, 2005.

[5]   Smalc, M., Shives, G., Chen, G., Guggari, S., and Norley, J., "Thermal performance of natural graphite heat spreaders," presented at Interpack 05-73073, San Francisco, CA, 2005.

[6]   Norley, J., Reynolds, A., Shives, G., and Smalc, M., "The development of natural graphite-based spreaders for reducing temperature and increasing temperature uniformity in flat panel displays," *SID 05 Digest, P-73*, pp. 562-565, 2005.

[7]   Boeuf, J. P., "Plasma display panels: physics, recent developments and key issues," *Journal of Physics D-Applied Physics*, vol. 36, pp. R53-R79, 2003.

[8]   Tovee, M. "An introduction to the visual system." Cambridge University Press. New York, NY. 1996.

[9]   K. -W. Whang and J. K. Kim, "Discharge Physics of Alternating Current Plasma Display Panels (PDPs)," Journal of Display Technology 1, 295-(2005)

[10]   Pitchford, L. "Plasma Display Panels." Coalition for Plasma Science. (CPAT), Toulouse, France.

[11]   Hutchinson, J. "The Plasma Behind the Plasma TV Screen." Plasma TV Science Organization. [Online] Available: http://www.plasmatvscience.org/theinnerworkings.html

[12]   Hutchinson, J. "The History of Plasma Display Panels." Plasma TV Science Organization. [Online] Available: http://www.plasmatvscience.org/plasmatv-history1.html

[13]   Zhang, S. "Vacuum-Ultraviolet/Visible Conversion Phosphors for Plasma Display Panels. IEEE Transactions on Plasma Science, Vol. 34, No. 2, April, 2006.

[14]   Kim, J.S., Park, Y.H., Choi, J.C., Park, H.L. "Temperature-Dependent Wmission Spectrum of $Ba_3MgSi_2O_8:Eu^{2+}$, Mn^{2+} Phosphor for White-Light-Emitting Diode." Electrochemical and Solid-State Letters, 8(8) H65-H67, 2005.

[15]   Bœuf, J.P. « Plasma Display Panels : Physics, Recent Developments, and Key Issues." Journal of Applied Physics. 36 (2003) R53-R79.

[16] Pitchford, L., Wang, J., Piscitelli, D., Boeuf, J.P. "Ion and Neutral Energy Distributions to the MgO Surface and Sputtering Rates in Plasma Display Panel Cells." IEEE Transactions on Plasma Science. Vol. 24, No. 2, pp. 351-359. April, 2006.

[17] Planar, INC. "Planar White Paper: Plasma Displays." November, 2005.

[18] Dawson, B., Ferguson, M., Marking, G., Diaz, A. L. "Mechanisms of VUV Damage in $BaMgAl_{10}O_{17}:Eu^{2+}$." American Chemical Society. Chem. Mater., 2004, 16, 5311-5317.

[19] Tae, H-S., Han, J-W., Jang, S-H., Kim, B-N., Shin, B-J., Cho, B-G., Chien, S-I., "Experimental Observation of Image Sticking Phenomenon in AC Plasma Display Panel." IEEE Transactions on Plasma Science. 2004.

[20] Shin, B. J., Choi, K. C., Tae, H. S., Seo, J. H., Kim, J. Y., Han, J. W. "Case Study on Temperature-Dependent Characteristics in AC PDPs." IEEE Transactions on Plasma Science. Vol. 33, No. 1, pp. 162-169, February, 2005.

[21] "Light and Vision." Department of Physics and Astronomy, Georgia State University. [Online] Available: http://hyperphysics.phy-astr.gsu.edu/hbase/hframe.html.

[22] "Samsung HP-P4621 42" HDTV-Ready-Flat-Panel Plasma TV." Product Features and Technical Details. www.samsung.com.

[23] Shooshtari, A., Kahn, J., Bar-Cohen, A., Dessiatoun, S., Ohadi, M., Getz, M., Norley, J. "The Impact of a Thermal Spreader on the Temperature Distribution in a Plasma Display Panel." ITherm, San Diego, CA, 2006.

[24] Kahn, J., Bar-Cohen, A. "Thermal Modeling and Luminosity Characterizatin of a Plasma Display Panel." HT2007-33834. ASME-JSME Thermal Engineering Summer Heat Transfer Conference. July 8-12, 2007, Vancouver, British Columbia, Canada.

[25] Fluent, "Fluent 6.2 Getting Started Guide," 6.2 ed. Lebanon, NH: Fluent, Inc., 2005.

[26] Incropera, F. P. and DeWitt, D. P., *Fundamentals of Heat and Mass Transfer*, 5th ed: John Wiley & Sons, 2002

[27] Lee, M., Pecht, M. G., and Lee, W., "Thermal assessment of glass-metal composition plasma display panels using design of experiments," *IEEE Transactions on Components and Packaging Technologies*, vol. 27, pp. 210-216, 2004.

[28] Ganter, R., Callegari, T., Pitchford, L. C., and Boeuf, J. P., "Efficiency of AC plasma display panels from diagnostics and models," *Applied Surface Science*, vol. 192, pp. 299-308, 2002.